

# Implementing plant hydraulics in the Community Land Model

Daniel Kennedy<sup>1</sup>, Sean Swenson<sup>2</sup>, Keith Oleson<sup>2</sup>, David Lawrence<sup>2</sup>, Rosie Fisher<sup>2</sup>, Pierre Gentine<sup>1</sup>

<sup>1</sup>Columbia

<sup>2</sup>National Center for Atmospheric Research, Table Mesa Drive, Boulder, Colorado, USA

## Key Points:

- A simplified soil-plant-atmosphere continuum model based on hydraulic theory is implemented in the Community Land Model (version 5).
- Prognostic leaf water potential replaces soil matric potential as the basis for stomatal conductance water stress.
- Prognostic root water potential is used to implement hydraulic root water uptake, replacing the heuristic soil ‘wilting’ factor .

**Abstract**

= enter abstract here =

**1 Introduction**

Trees face emerging climate change risk globally [Allen *et al.*, 2010; Anderegg *et al.*, 2013a]. In addition to stress from soil moisture drought, vegetation is susceptible to increasing atmospheric demand [Restaino *et al.*, 2016; Novick *et al.*, 2016a; Lemordant *et al.*, 2018]. Increases in vapor pressure deficit (VPD) have occurred with global warming [Ficklin and Novick, 2017; Seager *et al.*, 2015], and are associated with impacts on vegetation (e.g., large-scale die-off) [Williams *et al.*, 2013; McDowell and Allen, 2015]. Understanding vegetation response is a high priority, both for discerning climate impacts and for modeling feedbacks to the carbon and hydrological cycles. Significant uncertainty remains regarding how vegetation will respond to changes in hydroclimate within Earth System Models, feeding back onto the carbon cycle as vegetation mediates carbon uptake [De Kauwe *et al.*, 2017; Friedlingstein *et al.*, 2014; Trugman *et al.*, 2018].

Plant water stress parameterizations are important in Earth System Models, as they define vegetation regulation of surface fluxes (photosynthesis, transpiration) in response to water fluctuations. Vegetation water use strategies modulate carbon uptake, creating a critical coupling between the Earth System's carbon and hydrological cycles [Green *et al.*, 2017]. Drought stress parameterizations (functions which relate a metric of soil moisture status to leaf gas exchange) are widely used to define the response of stomatal conductance to vegetation water status, serving to attenuate transpiration, photosynthesis, and root water uptake with drying. The dynamics of this water stress representation in models have broad effects on critical land surface processes [Joetzjer *et al.*, 2014], such as photosynthesis rates. On daily and weekly time scales, water stress parameterizations influence the partitioning of latent versus sensible heat, modifying the Bowen ratio [Gentine *et al.*, 2007, 2011]. This in turn feeds back onto surface and air temperature, through land-atmosphere feedbacks [Bonan, 2008]. On longer timescales vegetation water use strategies regulate the global carbon and water cycles [De Kauwe *et al.*, 2015].

Several recent studies have aimed at advancing the representation of water flow through the Soil-Plant-Atmosphere continuum (SPAC) in land-surface and ecosystem models [Xu *et al.*, 2016; Christoffersen *et al.*, 2016; Sperry *et al.*, 2017]. Explicit modeling of water flow through the SPAC adds complexity, but is consistent with evidence of dynamic regulation of vegetation water use in response to both soil and atmospheric drying [Sperry and Love, 2015]. Furthermore, because they are based on Darcy's Law, SPAC models have a robust physical basis compared to empirical water stress formulations. SPAC models involve new parameters, which presents challenges [Drake *et al.*, 2017], but plant hydraulic trait data are available [Kattge *et al.*, 2011; Anderegg, 2015a], providing constraints on parameter estimation. Such data have been shown to be informative of species vulnerability to drought [Choat *et al.*, 2012]. Likewise vegetation water status observations are now available from remote sensing platforms, at a scale that is directly comparable to model development [Konings *et al.*, 2016; Grant *et al.*, 2016] and therefore can be used to validate model results [Momen *et al.*, 2017; Konings *et al.*, 2017b].

Specifically, the empirical representation of vegetation water stress in the Community Land Model (CLM) and other land surface models has been a known deficiency, with implications for the representation of the dry/wet season in tropical rainforests for example [Powell *et al.*, 2013; Ukkola *et al.*, 2016]. Indeed, recent studies suggest that the soil water stress parameterization introduces model bias in turbulent fluxes [Bonan *et al.*, 2014] and contributes to unrealistic drought response of photosynthesis and stomatal conductance [Powell *et al.*, 2013].

In this study, we develop a new plant water stress parameterization based on hydraulic theory within the recently released CLM version 5 (CLM5), which we refer to as the 'Plant Hydraulic Stress' (PHS) configuration.

Representing the SPAC introduces modeled vegetation water potential (discretized into leaf, stem and root elements) into the CLM, as well as an explicit representation of water supply, from the soil through the vegetation substrate. Transpiration is attenuated in the model with drought stress according to leaf water status, capturing dynamic vegetation water use regulation. These changes in the parameterization framework have numerous implications, including

1. Leaf water potential serves as a metric for water status compared to soil water or soil matric potential. As such, it reflects vegetation sensitivity to both soil and atmospheric drying, while serving as a diagnostic for excessive xylem tension and cavitation risk.
2. Modeling plant hydrodynamics allows representing hydraulic redistribution [Lee *et al.*, 2005], as the flow respects Darcy's law and thus is always directed down gradients of water potentials.
3. Further, root water potential can be used to predict gradient-based root water uptake based on Darcy's law, replacing the previous empirical transpiration partitioning heuristic. This provides the means to vary, for example, the mean depth of extraction with changing soil water conditions.
4. The new model can represent a range of water use strategies (i.e. isohydricity and anisohydricity), improving the connection between plant carbon allocation and water availability.
5. Modeling vegetation water potential allows improved connection to remote sensing observations of vegetation water status (Vegetation Optical Depth) [Konings *et al.*, 2016].

To assess the new model formulation, we carried out site-level simulations at Caxiuanã National Forest in Brazil, which features a critical biome (terra-firme moist tropical evergreen forest) [Fisher *et al.*, 2006]. Starting in 2001, a plot at this site was subjected to an approximately 50% percent precipitation through-fall exclusion. Due to the large drop in soil moisture at the precipitation exclusion site, significant vegetation water stress regulation of transpiration and photosynthesis was present at the site, providing a natural experiment to test the model [Fisher *et al.*, 2007].

In this paper we therefore: 1. Introduce the PHS theory and implementation in the CLM (Section 2) 2. Analyze the dynamics of modeled water stress, root water uptake and soil moisture profiles (Section 4) 3. Compare PHS to the behavior of the previous CLM water stress configuration (Section 5) 4. Discuss the benefits and limitations of the new model (Section 5.7)

## 2 Model Description

### 2.1 Photosynthesis

The CLM5 photosynthesis model is described in detail in Bonan *et al.* [2011], Thornton and Zimmermann [2007], and Oleson *et al.* [2013]. Photosynthesis is limited by three factors: Rubisco-limitations, light-limitations, and export-limitations following Farquhar *et al.* [1980] and Harley *et al.* [1992]. The implementation extends Sellers *et al.* [1996a,b] with co-limitation following Collatz *et al.* [1991].

The CLM5 photosynthesis module, in its default configuration, is a two-big-leaf model, with a sunlit and shaded leaf for each plant functional type [Thornton and Zimmermann, 2007; Dai *et al.*, 2004; Oleson *et al.*, 2013]. The canopy fluxes module iterates the solution

for leaf temperatures to satisfy the leaf surface energy balances on both sunlit and shaded leaves, in response to forcing conditions. Within this, the photosynthesis module further iterates to solve for stomatal conductance and intercellular CO<sub>2</sub> concentration, balancing stomatal flux of CO<sub>2</sub> with photosynthetic assimilation flux of CO<sub>2</sub>.

## 2.2 Stomatal Conductance

CLM5 implements the Medlyn stomatal conductance model, which reconciles the empirical and optimal approaches to stomatal conductance [Medlyn *et al.*, 2011]. The optimization aims to maximize photosynthesis relative to transpiration costs. Stomatal conductance of CO<sub>2</sub> ( $g_s$ ) is directly related to net photosynthesis ( $A_n$ ) and inversely related to the square root of the vapor pressure deficit near the leaf surface ( $\sqrt{D}$ ) and the concentration of CO<sub>2</sub> at the leaf surface ( $C_a$ ).

$$g_s = g_0 + \left(1 + \frac{g_1}{\sqrt{D}}\right) \frac{A}{C_a} \quad (1)$$

The model features two parameters  $g_0$  ( $\mu\text{mol} / \text{m}^2 / \text{s}$ ) and  $g_1$  ( $\text{kPa}^{0.5}$ ). The  $g_0$  parameter is minimum stomatal conductance, representing cuticular and epidermal losses (small). The  $g_1$  parameter relates to the marginal water cost guiding the optimization of carbon assimilation. These parameters are plant functional type dependent.

While maximizing assimilation relative to water transpiration costs ( $A - \lambda E$ ), the Medlyn model does not resolve concurrent limitations to stomatal conductance associated with declining soil water. To represent soil water stress, and its impact on leaf-gas exchange, land surface models typically include a ‘water stress factor’.

## 2.3 Water stress factor

In the CLM the water stress factor ( $f_w$ ) multiplies the ‘well-watered rate’ of maximum carboxylation ( $V_{\text{cmax,ww}}$ ) to effect water stress (as described in Oleson *et al.* [2013]).

$$V_{\text{cmax}} = f_w V_{\text{cmax,ww}} \quad (2)$$

Attenuating  $V_{\text{cmax}}$  is not the only method for incorporating a response to declining water availability. Other models opt to apply water stress directly to stomatal conductance, linking the stomatal conductance model slope parameter to soil moisture (e.g. De Kauwe *et al.* [2015]). However, Lin *et al.* [2018] found that only the intercept parameter was sensitive to soil moisture based on eddy-covariance observations. Furthermore Zhou *et al.* [2013] suggest that changes in assimilation tend to exceed those predicted by modulating  $g_1$  with soil moisture, but could be captured by changing  $V_{\text{cmax}}$ . Other field studies, however, suggest that measured  $V_{\text{cmax}}$  at the leaf level does not change with drought [Flexas *et al.*, 2004]. On the other hand, the modeled  $V_{\text{cmax}}$  is a bulk measure of  $V_{\text{cmax}}$  and may implicitly account for mesophyll conductance changes [Rogers *et al.*, 2017], which has been shown to be water stress dependent [Flexas *et al.*, 2012].

Uncertainty remains within the literature for how and where to apply water stress factors to photosynthesis and/or stomatal conductance [Zhou *et al.*, 2013; Novick *et al.*, 2016b; Sperry and Love, 2015]. For now, applying water stress through  $V_{\text{cmax}}$  seems well-supported, but future refinements may well be appropriate. In this study, we preserve the location of water stress used in CLM4.5, while experimenting with how  $f_w$  responds to environmental conditions.

### 2.3.1 Soil Moisture Stress (control model)

The control model for our study is Soil Moisture Stress (SMS), which we compare to the model of interest, Plant Hydraulic Stress (PHS). PHS is the default configuration of

CLM5. SMS is a re-configuration of CLM5, substituting in the CLM4.5 representations of (1) root water uptake (Section 2.4) and (2) water stress (described here). Otherwise PHS and SMS are identical.

In SMS, the scalar  $f_w$  is calculated as the summation of a soil wilting factor ( $w_i$ ) across the  $n$  soil layers, weighted by root fraction ( $r_i$ ) [Oleson *et al.*, 2013]. The soil wilting factor is a bounded linear function of soil matric potential ( $\psi_{\text{soil},i}$ ). The function is defined by two parameters, the soil potential with stomates fully open ( $\psi_o$ ) and fully closed ( $\psi_c$ ).

$$f_{w,\text{SMS}} = \sum_{i=1}^n r_i w_i \quad (3)$$

$$w_i = 0 \leq \frac{\psi_{\text{soil},i} - \psi_c}{\psi_o - \psi_c} \leq 1 \quad (4)$$

### 2.3.2 Plant Hydraulic Stress (new model)

PHS introduces a new formulation of  $f_w$ , which is based on leaf water potential ( $\psi_{\text{leaf}}$ ) instead of soil potential (described further in Section 2.5.2). The relationship is modeled with a sigmoidal function, subject to two parameters: the water potential at 50% loss of stomatal conductance ( $\psi_{50}$ ) and a shape-fitting parameter ( $c_k$ ).

$$f_{w,\text{PHS}} = 2 - \left( \frac{\psi_{\text{leaf}}}{\psi_{50}} \right)^{c_k} \quad (5)$$

Utilizing leaf water potential (instead of soil water potential) for drought stress introduces a new paradigm to the model. Leaf water potential is modulated by supply of sap to the leaves and by evaporative demand, as regulated by stomatal dynamics [Novick *et al.*, 2016b]. As a result, low soil water (bottom-up stress) induces stress due to limited water supply, but in addition, high atmospheric VPD can induce stress with the associated increases in the gradient in water potential across the plant xylem (top-down stress). This latter mechanism was absent from the previous water stress function (dependent on soil water potential only), by construction. Given the importance of rising VPD, it appears critical to include such mechanistic dependence of water stress. The new stress factor formulation reflects the concept of hydraulic safety, with vegetation avoiding excessive xylem tension associated with risk of cavitation. While the Medlyn stomatal conductance model does depend on VPD, this captures water ‘costs’ and not xylem tension.

## 2.4 Root Water Uptake

The CLM features a vertically discretized soil column with variable soil layer thicknesses. The number of soil layers ( $n$ ) can vary, depending on the depth to bedrock. Soil water movement in each soil layer is governed by Richards’ equation, with root water uptake ( $q_i$ ) incorporated as a sink term. Summed over the soil column, root water uptake is required to equal transpiration ( $T$ ).

$$T = \sum_i^n q_i \quad (6)$$

### 2.4.1 SMS

In the SMS configuration, a heuristic function is used to determine  $q_i$ . Transpiration is partitioned among the soil layers based on the product of the root fraction and the wilting factor, which must be normalized by  $f_w$ .

$$q_i = \frac{r_i w_i}{f_w} T \quad (7)$$

Substituting for  $w_i$  yields the SMS root water uptake equation as a function of the layer- $i$  soil potential ( $\psi_{\text{soil},i}$ ).

$$q_i = \begin{cases} 0 & \text{if } \psi_{\text{soil},i} < \psi_c \\ \frac{T}{f_w} \frac{r_i}{\psi_o - \psi_c} (\psi_{\text{soil},i} - \psi_c) & \text{if } \psi_c \leq \psi_{\text{soil},i} \leq \psi_o \\ \frac{T}{f_w} r_i & \text{if } \psi_c \leq \psi_{\text{soil},i} \leq \psi_o \end{cases} \quad (8)$$

In the Darcy framework, water fluxes are the product of hydraulic conductance ( $k_i$ ) and hydraulic gradient ( $\Delta\psi$ ). Upon inspection of (8), we can define hydraulic analogs resulting from the transpiration partitioning heuristic function, allowing easy comparison to the PHS root water uptake implementation.

$$\begin{aligned} q_i &= -k_i \Delta\psi \\ \Delta\psi &= \psi_c - \psi_{\text{soil},i} \\ k_i &= \frac{T}{f_w} \frac{r_i}{\psi_o - \psi_c} \\ \text{constrained by: } \Delta\psi &= \begin{cases} 0 & \text{if } \psi_{\text{soil},i} < \psi_c \\ \psi_c - \psi_o & \text{if } \psi_{\text{soil},i} > \psi_o \end{cases} \end{aligned} \quad (9)$$

#### 2.4.2 PHS

PHS installs an alternative to the SMS heuristic approach, using a mechanistic representation of root water uptake, following Darcy's Law. Instead of a constant parameter ( $\psi_c$ ) defining  $\Delta\psi$ , PHS installs a physical model of vegetation water potential (described in Section 2.5). The water flux from a given soil layer is driven by the gradient between soil potential ( $\psi_{\text{soil},i}$ ) and the water potential in the root collar ( $\psi_{\text{root}}$ ), after accounting for the effects of gravity ( $\rho g z_i$ , where  $z_i$  is the soil layer depth). Hydraulic conductance across the soil and roots ( $k_{sr}$ ) is modeled based on soil hydraulic properties and xylem vulnerability, accounting for both the path across the soil matrix and through the xylem conduits (details in Appendix zqz).

$$q_i = -k_{sr,i} (\psi_{\text{root}} - \psi_{\text{soil},i} + \rho g z_i) \quad (10)$$

### 2.5 Modeling Vegetation Water Potential

The PHS model within CLM5 uses Darcy's law to model the flow of water through the SPAC, which can be represented with an electrical circuit analogy (Figure 1). PHS solves for vegetation water potential along the path from soil-to-atmosphere. Vegetation water supply (root water uptake) and demand (transpiration) are both coupled to vegetation water potential, such that the solution for vegetation water potential is the set of values that matches supply with demand.

PHS solves for vegetation water potential at four locations:  $\psi_{\text{root}}$ ,  $\psi_{\text{stem}}$ ,  $\psi_{\text{shade-leaf}}$ , and  $\psi_{\text{sun-leaf}}$ . The number of nodes is chosen as the strict minimum to allow for differences in segment parameterizations [Simonin *et al.*, 2015; Sperry and Love, 2015], while also conforming to existing CLM model structure (vertically discretized soil layers, 2-big-leaf). At

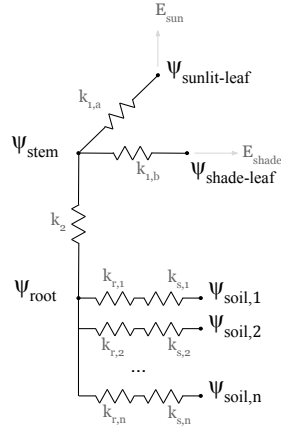


**Figure 1.** Plant hydraulic circuit analog schematic

each node in the circuit diagram in Figure 1 we model water potential, and, between nodes, we resolve the flux of water based on Darcy's law. Water uptake from the different soil layers is assumed to operate in parallel; a typical assumption justified by higher resistance in lateral versus central roots (e.g. *Williams et al.* [2001]). Two resistors operate in series between each  $\psi_{\text{soil}}$  and  $\psi_{\text{root}}$ , to represent the path across the soil matrix and then through the root tissue [*Williams et al.*, 1996]. Specifics on the parameterization of hydraulic conductance for each segment are provided in Appendix B.1.

### 2.5.1 Water supply

Water supply is modeled via Darcy's Law, where flux of water ( $q$ ) is the product of the path hydraulic conductance ( $k$ ) and the gradient in water potential ( $\psi_2 - \psi_1$ ) after accounting for gravitational potential ( $\rho g \Delta z$ ). Equation 11 represents the flow from a generic node 1 to node 2.

$$q = -k (\psi_2 - \psi_1 + \rho g \Delta z) \quad (11)$$

For simplicity, PHS does not represent plant tissue water storage (or capacitance, using the electrical circuit analogy), which is in line with recent supply-loss theory [*Sperry and Love*, 2015]. Capacitance significantly complicates the water potential solution [*Celia et al.*, 1990] and is challenging to parameterize [*Bartlett et al.*, 2016]. However, buffering of water stress provided by tissue water storage could potentially be important especially on sub-daily timescales [*Meinzer et al.*, 2009; *Epila et al.*, 2017], whereby its inclusion may be warranted in future model generations.

Hydraulic conductance through vegetation segments is modeled following empirical xylem vulnerability curves [*Tyree and Sperry*, 1989], where segments lose conductance with increasing xylem tension related to cavitation and embolism [*Holbrook et al.*, 2001]. The vulnerability curves model loss of conductance relative to maximum conductance ( $k_{\text{max}}$ ) using two parameters:  $c_k$ , a sigmoidal shape-fitting parameter, and  $p_{50}$ , the water potential at 50% loss of segment conductance (following *Gentine et al.* [2016]).

$$k = k_{\text{max}} 2^{-\left(\frac{\psi_1}{p_{50}}\right)^{c_k}} \quad (12)$$

Both  $c_k$  and  $p_{50}$  can be estimated from field experiments [Sack *et al.*, 2002], and  $p_{50}$  is available in the TRY trait database [Kattge *et al.*, 2011]. Parameterization based on  $p_{50}$  aligns with the call for a transition to models that use a wider range of plant functional trait data in their parameterization [Anderegg, 2015a]. The loss of xylem conductivity is based on lower terminal water potential ( $\psi_1$ ) as is typical in other simplified models [Xu *et al.*, 2016], but may underestimate the integrated loss of conductivity [Sperry and Love, 2015].

PHS models root, stem, and leaf tissue conductances according to equation 12. The parameterization of  $k_{\max}$  varies by hydraulic segment (see details in Appendix B1). The conductance across the soil matrix to the root surface follows Williams *et al.* [2001] and Bonan *et al.* [2014]. Bulk soil resistivity is based on Clapp and Hornberger [1978] as described in Oleson *et al.* [2013]. Details are provided in Appendix B1.

### 2.5.2 Water demand

Water demand is calculated using the Medlyn stomatal conductance model (see Section 2.2) modulated by the CLM water stress factor. As discussed earlier  $f_w$  is based on leaf water potential in PHS, where stress increases as leaf water potential becomes more negative [Klein and Niu, 2014]. Because leaf water potential is modeled separately for sunlit and shaded leaves,  $f_w$  takes on distinct sunlit and shaded values.

$$\begin{aligned} f_{w,sun} &= 2 \left( \frac{\psi_{\text{sun-leaf}}}{\psi_{50}} \right)^{c_k} \\ f_{w,shade} &= 2 \left( \frac{\psi_{\text{shade-leaf}}}{\psi_{50}} \right)^{c_k} \end{aligned} \quad (13)$$

Shaded and sunlit leaf transpiration ( $E_{\text{sun}}$ ,  $E_{\text{shade}}$ ) are calculated by attenuating maximal transpiration ( $E_{\text{sun,max}}$ ,  $E_{\text{shade,max}}$ ) according to  $f_w$ .  $E_{\text{sun,max}}$  and  $E_{\text{shade,max}}$  are calculated at the beginning of each timestep by running the stomatal conductance model with  $f_w = 1$ . Equations (13) and (14) reflect a simplification used within iterations of the PHS module, neglecting non-linear components of the relationship between stress and transpiration (described further in Section zqz).

$$\begin{aligned} E_{\text{sun}} &= f_w E_{\text{sun,max}} \\ E_{\text{shade}} &= f_w E_{\text{shade,max}} \end{aligned} \quad (14)$$

### 2.5.3 PHS solution

PHS solves for the set of vegetation water potential values ( $\psi$ ) that matches water supply (root water uptake) to water demand (transpiration), while satisfying continuity across the four water flow segments (soil-to-root, root-to-stem, stem-to-leaf, and leaves-to-transpiration). Beginning from an initial condition of  $\psi$  (from the previous timestep), PHS computes the flux divergence  $f$  (representing the mismatch of flow in and out of each segment) and iteratively updates  $\psi$  until  $f \rightarrow 0$ .

$$\psi = \begin{bmatrix} \psi_{\text{sun}} \\ \psi_{\text{shade}} \\ \psi_{\text{stem}} \\ \psi_{\text{root}} \end{bmatrix} \quad (15)$$

$$f(\psi) = \begin{bmatrix} E_{\text{sun}} - q_{\text{sun}} \\ E_{\text{shade}} - q_{\text{shade}} \\ q_{\text{sun}} + q_{\text{shade}} - q_{\text{stem}} \\ q_{\text{stem}} - \sum_{j=1}^n q_{\text{root},j} \end{bmatrix} \quad (16)$$



$$A = \frac{df}{d\psi} \quad (17)$$

While  $|f| > 0$

$$\begin{aligned} \Delta\psi &= A^{-1} f(\psi_i) \\ \psi_{i+1} &= \psi_i + \Delta\psi \end{aligned} \quad (18)$$

The numerics are tractable because  $f$  has continuous, analytical derivatives and  $A$  (a 4x4 matrix with six null entries) is easy to invert when well-conditioned. Supply and demand converge, because transpiration demand decreases with more negative leaf water potentials and supply increases with more negative leaf water potentials. The PHS loop is nested within iterations for intercellular  $\text{CO}_2$  concentration and leaf temperature. As described earlier, within a set of PHS iterations (18), transpiration is assumed to be linear with  $f_w$ . The non-linear relationship between  $f_w$  and transpiration is resolved through iteration for converging  $f_w$  alongside intercellular  $\text{CO}_2$ . Details on the numerical implementation are provided in Appendix Section B.1.

### 3 Experiment Description

We use a set of four simulations to assess the impact of the plant hydrodynamics model (PHS vs. SMS) on a throughfall exclusion experiment.

1. SMS, with ambient throughfall conditions (AMB)
2. SMS, with 60% of throughfall excluded (TFE)
3. PHS, AMB
4. PHS, TFE

All four simulations use the same version of CLM5 (development version r270, [www.github.com/ESCOMP/ctsm/releases/tag/clm4\\_5\\_18\\_r270](https://www.github.com/ESCOMP/ctsm/releases/tag/clm4_5_18_r270)), which features a switch that can toggle between SMS and PHS configurations. Simulations are run offline (uncoupled from an active atmospheric model), spanning from 2001 through 2003, utilizing the satellite phenology (SP) mode of CLM5 in which vegetation state (LAI, canopy height) is prescribed and biogeochemistry is inactive. Six-year spin-up simulations (one each for SMS and PHS) are used to create initial conditions, repeating the Ambient simulation twice. Descriptions of site characteristics, forcing data, and observational sap flux and soil moisture, can be found in *Fisher et al. [2007]* and *Fisher et al. [2008]*.

#### 3.1 Parameter Values and Throughfall Exclusion

Parameter values concerning vegetation hydrodynamics are presented in Table 1. All other parameters use the default values associated with the r270 version of CLM5. Informed by parameter values reported in *Fisher et al. [2008]*, we tuned soil hydraulic parameters and throughfall exclusion rates to get in range of observed soil moisture (Supp Fig A.6). A 972-member ensemble of simulations was used to tune the parameters for the PHS configuration to fit sap flux observations (see Appendix B.4). No tuning was used for the SMS configuration.

## 4 Results

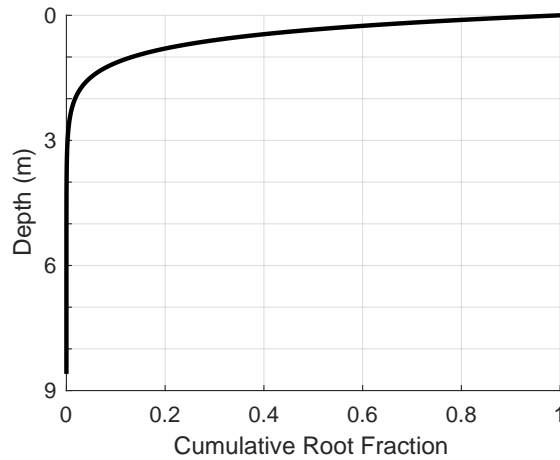
### 4.1 Vegetation water potential

Under ambient conditions, 2003 dry season (September-October-November) model average sunlit leaf water potential is -1.65 MPa at midday (local time 12-14h, Figure 3a). The midday pressure drop is primarily between  $\psi_{root}$  and  $\psi_{stem}$ , representing the root collar

310

**Table 1.** Select parameter values

CLM name	Full Name	Symbol	Value
kmax(1)	Maximum Sun Branch Conductance	$k_{1a,max}$	$4e-8 s^{-1}$
kmax(2)	Maximum Shade Branch Conductance	$k_{1b,max}$	$4e-8 s^{-1}$
kmax(3)	Maximum Stem Conductivity	$k_{2,max}$	$4e-8 m/s$
krmax	Maximum Root Conductivity	$k_{r,max}$	$6e-9 m/s$
psi50	Water potential at 50% loss of conductivity	$\psi_{50}$	-1.75 MPa
ck	Vulnerability shape parameter	$c_k$	2.95
smpso	Soil potential with stomata fully open	$\psi_o$	-0.65 MPa
smpsc	Soil potential with stomata fully closed	$\psi_c$	-2.5 MPa
medlyn_intercept	Medlyn intercept	$g_0$	$100 \mu mol / m^2 / s$
medlyn_slope	Medlyn slope	$g_1$	$6 kPa^{0.5}$
n	Soil porosity to 4.64 meters	$n$	0.42
n	Soil porosity beyond 4.64 meters	$n$	0.28
hksat	Saturated soil hydraulic conductivity	$k_{s,max}$	$3e-5 m/s$
sucsat	Saturated soil matric potential	$\psi_{sat}$	461 Pa
bsw	Brooks-Corey parameter	$b$	6



318

**Figure 2.** Cumulative rooting distribution

324

and upper stem, respectively. Under TFE, model midday leaf water potential decreases to -2.31 MPa (Figure 3b). Partitioned among the segments of the SPAC, the changes in leaf water potential (totaling -0.66MPa) due to TFE are: -0.44MPa soil potential, -0.66MPa soil-to-root, +0.45MPa root-to-stem, and -0.001MPa stem-to-leaf. This comports with previous evidence that seasonal changes in hydraulic resistance are larger belowground [Fisher *et al.*, 2006].

329

330

331

332

333

334

335

336

337

338

Modeled root water potential values match wet season observations, but are less negative than dry season observations under ambient conditions [Fisher *et al.*, 2006]. Midday leaf water potential features a seasonal cycle, with lower values during the dry season (Figure 3c). Modeled leaf water potential values under ambient conditions are less negative than averages reported by Fisher *et al.* [2006] (1.71 MPa during the wet season and -2.47 MPa during the dry season), but are within the range of observations. The model seems to underestimate isohydricity (i.e. minimal leaf water potential drop during drought) in response to TFE, showing a drop in leaf water potential of 0.66MPa (dry season, 2003), whereas observations showed no significant difference [Fisher *et al.*, 2006].

**Table 2.** Root-zone soil potential <sup>a</sup> (MPa) terciles for Figure 5

Simulation	T1	T2
SMS, Ambient	-0.01	-0.54
SMS, TFE	-0.29	-1.74
PHS, Ambient	-0.01	-0.05
PHS, TFE	-0.05	-0.33

<sup>a</sup>SMS values correspond to daily mean root-fraction weighted soil potential. PHS values correspond to predawn root water potential.

## 4.2 Stress factor

Average midday stress values are comparable during the 2003 dry season (Figure 4) between the two model configurations. Under ambient conditions, the average stress factor values are 0.59 and 0.54 for SMS and PHS, respectively (dry season, midday), decreasing to 0.16 and 0.21, with TFE. While the SMS stress factor has minimal diurnal variability (Figure 4a), PHS features increased stress at midday (Figure 4b), corresponding to the drop in leaf water potential (Figure 3b,c). Indeed, the PHS stress factor responds to both soil moisture and VPD (Figure 5c,d), while SMS responds only to soil moisture (Figure 5a,b). This dependence on VPD results in more wet season (February-March-April) stress with PHS (as compared to SMS) under both ambient and TFE conditions (Figure 6a-d).

## 4.3 GPP and Transpiration

The two models predict similar total GPP across 2002-2003 under TFE, with 3.96 kg/m<sup>2</sup> for SMS and 4.00 kg/m<sup>2</sup> for PHS, but GPP is lower for PHS under ambient conditions (4.86 kg/m<sup>2</sup>) as compared to SMS (5.46 kg/m<sup>2</sup>, Figure 6e-h). Seasonal variability in GPP is smaller with PHS. The standard deviations of daily GPP (2002-2003) are 0.49 and 1.55 g/m<sup>2</sup>/d for AMB/TFE, as compared to 1.53, 2.73 g/m<sup>2</sup>/d with SMS. Transpiration seasonality is present in both models (Figure 7a,b), but with a larger amplitude for SMS. PHS yields a better fit to field observations of daily sap flux, with higher R<sup>2</sup> and lower RMSE compared to SMS (R<sup>2</sup>: [AMB] 0.742 vs. 0.434; [TFE] 0.449 vs. 0.303; RMSE: [AMB] 0.508 vs. 0.764; [TFE] 0.741 vs. 1.026) under both ambient and TFE conditions (Figure 7c-f).

## 4.4 Root water uptake: dynamics

Root water uptake is more sensitive to soil potential with PHS (Figure 8), which follows from sharp declines in hydraulic conductance with drying. Hydraulic conductance decreases approximately by three orders of magnitude across the range of PHS soil potential (Supp Figure A.3b). In contrast, the SMS-implied conductance increases with more negative soil potentials, until  $\psi_{\text{soil}}$  reaches -2.5MPa, beyond which it is defined to equal 0 (Supp Figure A.3a). Root water uptake still decreases with SMS as soils dry, but only because of the decrease in  $\Delta\psi$  (Supp Figure A.4c). Whereas PHS imparts a diurnal cycle to root water uptake via dynamic root water potential, the hydraulic gradient with SMS is defined by  $\psi_c$ , which is constant, requiring a diurnal cycle in the (implied) hydraulic conductance (Supp Figure A.4).

## 4.5 Root water uptake: profiles

Overall, the two model configurations feature comparable transpiration during the dry season under ambient conditions (PHS: 28.3cm, SMS: 28.5cm). However they feature distinct vertical profiles, as PHS removes less water from intermediate soil layers (0.5-1.5meters)

(Figure 9d). SMS removes more water from these layers, due to the lower sensitivity of root water uptake to soil potential. Likewise, partitioning of root water uptake within the soil column is more sensitive to precipitation in PHS (Figure 9a-c). In PHS, during the longer periods without rain, surface extraction plateaus and transpiration is fueled by the deeper soil water. After rain events, surface extraction renews, while at depth, root water fluxes reverse, with water deposited instead of being extracted. Both models decrease surface extraction under TFE (Figure 9b), but PHS has a larger compensation from beyond 2m (Figure 9c), allowing more overall transpiration (14.6 vs. 10.8 cm).

During the wet season PHS utilizes more water from the near-surface soil layers (Figure 10b), with zero net root water uptake beyond soil depth of 35.2 cm in ambient conditions (or beyond 9.6cm under TFE). SMS extracts 49.8% (AMB) and 81.5% (TFE) of total transpiration from beyond those levels (Figure 10). PHS does extract some water from beyond 35.2/9.6cm into the soil profile, but in service of hydraulic redistribution, sending the extracted water deeper into the soil column.

#### 4.6 Hydraulic redistribution

SMS precludes hydraulic redistribution (HR) setting root water uptake to zero when reversed gradients in water potential occur (contrary to PHS). With PHS, HR totals to 38.9 cm under ambient conditions and 40.0 cm under TFE over the course of 2003, with the majority (28.0, 26.7 cm) of this HR occurring at night (Figure 11). HR occurs in both directions (Supp Fig A.5), but is predominately downwards (AMB: 30.7cm, TFE: 33.8cm). Likewise HR occurs during both the wet and dry seasons. The seasonality changes with TFE, as AMB has more HR during Sept-Jan, while TFE features more HR during Feb-Apr.

#### 4.7 Soil moisture

During the dry season, SMS simulations yield much lower values for soil matric potential (Figure 12, Supp Fig A.6). SMS root-fraction-weighted average soil potential is -1.42 MPa under ambient conditions (dry season), compared to -0.14 MPa with PHS (average predawn root water potential). With TFE, SMS dry season soil potential drops to -2.51 MPa and PHS to -0.50 MPa.

PHS better matches observations of soil moisture, with RMSE lower by up to 55% (Figure 13, Supp Fig A.7). The SMS values correspond to a significant dry bias (Figure 13), especially in the first meter of the soil column. This is associated with the soil wilting parameter ( $\psi_c$ ), which takes the value -2.5MPa for the broadleaf evergreen tropical PFT [Oleson *et al.*, 2013].

#### 4.8 Soil moisture effect on transpiration

Model soil potential shows limited relationship to sap flux observations under ambient conditions (Supp Fig A.8b,f). However, in the SMS configuration, modeled transpiration decreases strongly with more negative soil potential (Supp Fig A.8a), biasing the model relative to observations (Fig 14a).

Sap flux observations under TFE show a stronger relationship with soil potential especially with PHS (Supp Fig A.8h,d). With SMS, the modeled attenuation of transpiration with soil potential again seems to bias modeled transpiration (Fig 14b). Derived from  $\psi_c$ , transpiration approaches zero when soil potential reaches -2.5 MPa (Supp Fig A.8c). The two PHS simulations feature less structure in transpiration bias vs. soil potential and less bias overall (Fig 14c,d).

## 5 Discussion

### 5.1 The promise of plant hydraulics

Plant hydraulics can potentially improve model predictions of vegetation response to climate change [Sperry and Love, 2015], especially if parameter ranges and model complexity can be constrained [Rogers *et al.*, 2017]. Numerous site-level models have deployed plant hydraulics (e.g. Williams *et al.* [1996]; Sperry *et al.* [1998]; Bohrer *et al.* [2005]), and studies show vegetation water potential can improve predictions of stomatal response to the environment [Sperry *et al.*, 2017; Anderegg *et al.*, 2017]. More recently hydraulics have been coupled to global models [Bonan *et al.*, 2014; Xu *et al.*, 2016; Christoffersen *et al.*, 2016], but most Earth System Models do not provide a mechanistic representation of vegetation water dynamics.

In this study, we have implemented plant hydraulic theory within CLM5, using dynamic vegetation water potential to modulate leaf gas exchange and root water uptake. PHS installs a model for predicting vegetation water potential by extending Darcy's Law through the vegetation substrate (Figure 1), which introduces 4 new variables to the model ( $\psi_{\text{root}}$ ,  $\psi_{\text{stem}}$ ,  $\psi_{\text{shade-leaf}}$ , and  $\psi_{\text{sun-leaf}}$ ). The model is able to capture expected diurnal and seasonal dynamics of vegetation water potential, with lower values within the stem and leaves at mid-day and during the dry season (Figure 3). The bulk of our analysis and discussion pertains to how these vegetation water potential variables can be used to improve the representation of transpiration, root water uptake, and soil moisture dynamics within the CLM.

Support for hydraulic models include improvements in modeling mortality and productivity [McDowell *et al.*, 2018; Choat *et al.*, 2012]. However, concerns exist in the literature regarding hydraulic model complexity and parameterization [Verhoef and Egea, 2014; Drake *et al.*, 2017], which led to a series of simplifications implemented in our model design (see Section 2). Recent work suggests model complexity can be managed, given the significant coordination of hydraulic traits [Bartlett *et al.*, 2016; Christoffersen *et al.*, 2016]. Furthermore incorporating plant hydraulics provides access to new streams of observational data for model validation and parameterization. Vegetation water potential can be monitored in the field [Boyer, 1967] and has been shown to correlate with microwave remote sensing products [Momen *et al.*, 2017]. Parameter values can be measured in the field [Sack *et al.*, 2002] and are available in the TRY database [Kattge *et al.*, 2011].

### 5.2 Water stress and stomatal conductance

PHS models (sunlit and shaded) leaf water potential, which serves as the input to the water stress factor, replacing the previous version based on soil water potential (SMS). This imparts a diurnal cycle to the water stress factor (Figure 4), following the midday drop in leaf water potential induced by leaf-level VPD transpiration demand. As such, stress now depends on transpiration demand, and, in turn, leaf-level VPD and radiation (Figures 5,A.2). This water stress implementation tries to capture xylem tension stress, where vegetation must limit transpiration to avoid cavitation and embolism. This is in addition to the VPD response of the Medlyn stomatal conductance model (replaced Ball-Berry in the updates from CLM4.5 to CLM5), where stomatal conductance is proportional to  $\text{VPD}^{-0.5}$ , which optimizes carbon gain versus water losses [Medlyn *et al.*, 2011]. Support for a hydraulics-based stress implementation exists in the literature [Novick *et al.*, 2016b; Sperry *et al.*, 2017], but the field has not yet reached a consensus on the best functional form for this type of water stress [Zhou *et al.*, 2013].

The PHS water stress factor exhibits a seasonal cycle, with lower values (indicating more stress) during the dry season. However, the seasonal variation in water stress is smaller than with the control model (Figure 6a-d). As a result PHS features less seasonal variability in GPP, especially under ambient conditions (Figure 6e-h). The PHS water stress factor induces a negative feedback on GPP. Factors increasing GPP (e.g. more light) also increase

xylem tension and stress, which opposes increases in GPP. *Restrepo-Coupe et al.* [2017] show that GPP increases at Caxiuanã during the dry season, suggesting that PHS may improve the GPP seasonal cycle relative to the control model.

PHS underestimates the seasonal cycle in transpiration under ambient predictions, and exhibits less seasonal variability than sap flux observations (Figure 7a,c). Both models produce a high bias in transpiration under TFE, similar to previous evidence showing that models tend to underestimate the effect of TFE [Powell et al., 2013]. Further work could compare the various permutations of water stress proposed in the literature, and/or concurrent improvement in photosynthesis parameters and model structure. Because considerable uncertainty remains regarding the appropriate functional form of water stress, PHS should be considered a starting point for improving transpiration response to hydroclimate. In our experiment, PHS does improve transpiration predictions, with lower RMSE and higher correlation compared to the control model, albeit with the advantage of model tuning (Figure 7).

### 5.3 The extensive influence of $\psi_c$

[will be removed]

[as pierre has noted, this section doesn't really work on its own, I'm currently working to incorporate the main points into the other sections]

Whereas the previous two subsections discuss model transpiration and water stress, the next four subsections pertain to the dynamics of root water uptake and soil moisture. In the SMS model configuration, these dynamics are strongly influenced by  $\psi_c$ , the soil potential at which stomates are fully closed. For the Broadleaf Evergreen Tropical PFT (BET),  $\psi_c$  equals -2.5 MPa [Oleson et al., 2013].

Root water uptake shows a strong dependence on  $\psi_c$ , defined to approach 0 as  $\psi_{\text{soil}}$  nears  $\psi_c$  (Figure 8a,b). As such,  $\psi_c$  sets the intercept for the relationship between root water uptake and  $\psi_{\text{soil}}$ . The maximum root water uptake is determined by transpiration dynamics and the layer root fraction. The onset of stress, where the curve begins to decline from maximal root water uptake, is defined by the soil potential with stomates fully opened,  $\psi_o$ , which equals 0.66MPa for BET.

Root water uptake from a given soil layer is defined to be zero whenever soil potential is more negative than  $\psi_c$  (Figure 8), following from the definition of the SMS water stress factor (Section zqz). This sharp non-linearity tends to make soil potential decrease to and then hold at values equal to  $\psi_c$  (Figure 12). As such,  $\psi_c$  has strong influence on model output for both transpiration and soil moisture, despite limited empirical or physical basis [Rogers et al., 2017].

### 5.4 Structural improvements in modeling root water uptake

Whereas the previous two subsections discuss model transpiration and water stress, the next three pertain to the dynamics of root water uptake and soil moisture. PHS uses dynamic root water potential ( $\psi_{\text{root}}$ ) as the sink for measuring the hydraulic gradient governing root water uptake (Figure 3). Because SMS does not resolve water potential through the vegetation substrate, the model uses a constant parameter,  $\psi_c$  to define the hydraulic gradient. As such, PHS provides a critical structural improvement for modeling root water uptake, consistent with extensive evidence of dynamic vegetation water potential (e.g. *Fisher et al.* [2006]).

Root water uptake is equal to the product of  $\Delta\psi$  and hydraulic conductance  $k$ . The conductance varies by soil layer and, with PHS, features mechanistic reductions based on root xylem vulnerability and soil hydraulic properties, as is appropriate for hydraulic-based models [Cai et al., 2014; Warren et al., 2015]. As a result the soil-root conductance features



a strong, positive relationship with soil potential, decreasing by almost three orders of magnitude as the soil dries (Supp Fig A.3). Hydraulic conductance is not explicitly modeled with SMS, but the values implied by the transpiration partitioning function (see Section 2.4.1), actually increase as soils dry over the domain of  $\psi_c < \psi_{\text{soil}} < \psi_o$  (Supp Fig A.3).

Furthermore, whereas SMS uses a relative notion to scale uptake by root abundance (root fraction), PHS opts for an absolute measure (root area), which can better capture dynamic allocation decisions in response to drying. With SMS, if root mass were to double in every soil layer, the root fraction remains unchanged, yielding no advantage in accessing soil water. With PHS, as root area in a soil layer increases so does the hydraulic conductance, even if the layer root fraction remains constant.

PHS appropriately penalizes extraction from depth, due to increasing distance between roots, increasing xylem length, and contributions from gravity (all missing from SMS). As a result, PHS favors surface extraction when water is available (Figure 10). The model can overcome these penalties, with compensatory root water uptake observed with increased extraction from beyond 2 meters depth during the TFE dry season (Figure 9). Dynamic root water potential (and conductance) gives the system more play, allowing the model to switch root water uptake to the lower layers as the surface dries out.

PHS also eschews the unsubstantiated constraints on  $\Delta\psi$  imposed by SMS ( $0 \geq \Delta\psi \geq \psi_c - \psi_o$ , see Section 2.3.1). Allowing  $\Delta\psi$  to change sign yields a representation of hydraulic redistribution, which has been observed in Amazonian forests [Oliveira *et al.*, 2005].

## 5.5 Hydraulic Redistribution (HR)

In our experiment, modeled HR totals to 38.9 cm over the course of 2003 under ambient conditions and 40.0 cm with TFE (Figure 11). HR occurs in both directions vertically (Supp Fig A.5), consistent with field observations [Burgess *et al.*, 1998]. Modeled HR is mostly downwards, sending water shallower water from rain events deeper into the soil column and thus saving it for when it is most needed, i.e. dry season. This would seem to convey an advantage to deep-rooted individuals, banking water for later use out of reach of shallow-rooted competitors. HR can offer significant water subsidies during dry periods [Jackson *et al.*, 2000] and has been highlighted as an important missing feature in CLM [Lee *et al.*, 2005].

Some of the challenges we faced were that HR seemed to oversupply the top layer of the soil column (spanning 0 to 2 cm below ground) and thus significantly degraded modeled soil evaporation (not shown). In lieu of this, we set the hydraulic conductance to zero in that uppermost layer, disallowing any root water uptake there. Furthermore, observations of HR are extremely difficult, and the degree to which HR actually occurs is unclear. Unequivocal detection of HR involves the observation of reverse flow along transport roots, typically at rates close to the detection threshold of sap flow monitoring systems. In our simulations, HR increases root water uptake by up to 52% relative to transpiration alone (2003, TFE).

HR follows directly from Darcy's Law, occurring when water potential in a given soil layer is more negative than  $\psi_{\text{root}}$ , but it remains to be seen whether HR as modeled in this implementation is a feature or a liability. PHS may overestimate HR, given the simplified root system architecture [Bouda and Saiers, 2017] and the lack of an explicit representation of fine-root cavitation [Kotowska *et al.*, 2015]. Other models, similar to the SMS paradigm, disallow HR by constraining root water uptake to be positive [Xu *et al.*, 2016]. We view this first implementation of HR into the default versions of the CLM as a 'null' hypothesis for the functioning of this process, and as a platform to allow further refinement from the plant hydraulics community. Isotopologues of water could be used as a tool to further constraint this redistribution in CLM in the future.

## 5.6 Soil moisture and its influence on transpiration

Partly due to HR, vertical and temporal gradients in soil potential are significantly reduced in PHS (Figure 12). This is also related to the root water extraction gradient, which is significantly smaller in PHS (Supp Fig A.4). The SMS sink potential ( $\psi_c$ , -2.5MPa), is significantly lower than PHS ( $\psi_{\text{root}}$ , Figure 3). This is associated with a significant dry bias relative to observations in the SMS simulations, especially in the first meter of the soil column. PHS reduces soil moisture RMSE by up to 55% relative to SMS (Figure 12).

The relationship with soil water potential seems to bias SMS predictions of transpiration relative to sap flux observations (Figure 14a,b). Under ambient conditions, soil water shows little relationship with sap flux observations with either model configuration (Figure A.8b,f), but SMS modeled transpiration decreases strongly in response to soil drying. This is in line with *Bonan et al.* [2014], where the water stress factor was found to impose too much attenuation of transpiration. PHS features less structure in the relationship between transpiration bias and soil potential and less bias overall (Figure 14c,d). Likewise PHS yields a stronger relationship than SMS between soil potential and sap flux observations during TFE (Figure A.8b,f). This represents a major development, given repeated calls to improve vegetation water stress in the next generation of terrestrial biosphere models [*Powell et al.*, 2013; *Rogers et al.*, 2017].

## 5.7 Benefits and limitations of PHS

[need to rewrite this]

Modeling stomatal conductance and photosynthesis, especially subject to water stress, is an area of ongoing research. We use the Medlyn VPD-dependence model coupled to a hydraulic stress function that attenuates  $V_{\text{cmax}}$ . This complies with observations [*Lin et al.*, 2018; *Zhou et al.*, 2013] that stress applied through  $g_1$  underestimates attenuation of photosynthesis. However, there is no direct evidence of declines in  $V_{\text{cmax}}$  at the leaf level with drought [*Flexas et al.*, 2006], whereby future work may seek to represent mesophyll conductance in CLM to correct such discrepancy.

The model hydraulic supply representation is simplified, to reduce the model parameter and computational burdens. No capacitance. No integration of xylem or soil conductances vulnerability, instead based on lower node. No hysteresis in loss of conductance, xylem instantly regain conductance upon re-wetting. Leaf conductance simplified. Soil layers fully parallel, soil potential constant each time step.

Parameter uncertainty is significant. Notions of hydraulic architecture will never perfectly fit on this modeling scale, especially in a PFT paradigm. Field measurements of hydraulic traits will help constrain parameter ranges, but mostly only aboveground. Flux observations can help to tune stress parameters. Parameter estimation for root functioning is significantly more challenging, given the difficulty in underground trait observations. Likewise observational constraints of vertically-resolved states and fluxes underground are scarce. Follow-up work will be geared towards parameter estimation and assessing model skill.

## 5.8 Inconsistencies in SMS

[I plan to delete this section, after double-checking that the main points are covered either in the model description or the previous discussion sections.]

### 5.8.1 Constant pulling potential

With SMS, the water potential gradient is implicitly defined for each soil layer as the difference between the soil water potential in that layer ( $\psi_i$ ) and a constant parameter, the soil



water potential when stomata are fully closed ( $\psi_c$ ). This parameter serves as the vegetation “pulling” potential for calculating the soil transpiration sink.

Using a constant wilting point is inconsistent with extensive evidence from the field of dynamic vegetation water potential, and cohesion tension theory (CITATIONS NEEDED) driving the transpiration flow. Likewise the values for  $\psi_c$  are quite negative, (-2.5 MPa for broadleaf evergreen tropical, BET, forests). *Fisher et al.* [2006] measured midday stem potential consistently higher than -0.5 MPa during the wet season, and on average -1.69 and -1.53 MPa during the dry season in the control and exclusion plots, respectively.

### 5.8.2 Conductance dynamics

In SMS, in lieu of dynamic vegetation water potential, intra-day SMS soil sink dynamics derive from a highly variable conductance (CLARIFY). As inferred in Equation 9, SMS conductance is modeled as a function of  $T_{max}$ , and three constant parameters.  $T_{max}$  is highly dynamic, responding to the diurnal course in transpiration demand. This is inconsistent with general principles of porous media flow, where conductivity is a function of the hydraulic architecture and its wetted status. Likewise, this representation of conductance does not represent the characteristic phenomenon where vessels lose conductance with drying.

### 5.8.3 No dependence on belowground carbon allocation

As is typical in water stress parameterizations, the SMS conductance is scaled by layer using an area basis, here using the relative vertical root fraction is used. With PHS, an absolute measure of root biomass is used (see Appendix Equation B.7), so that the belowground water cycle interacts with carbon allocation to the roots. An absolute measure better conforms with the physics of porous media flow and better responds to varying carbon allocation strategies. For example, with SMS, if root mass doubles in every soil layer, the root access to water remains unchanged.

### 5.8.4 Lacks penalties for extraction from depth

Both PHS and SMS account for the effect of decreasing root area with depth (PHS, root area; SMS, root fraction), but PHS implements two other penalties for extracting water from deep in the soil column that are missing from SMS. The first is minor, but water extracted from depth must overcome gravity, amounting to about 0.01 MPa per meter in depth. This is missing from SMS and included with PHS. Likewise, SMS ignores the fact that hydraulic conductance is generally taken to scale with the inverse of conducting length. Deeper roots feature longer root tissue conducting length, and root spacing within the soil is less dense, requiring longer conducting distances across the soil matrix. In PHS, both these processes result in diminished hydraulic conductance (UNCLEAR).

### 5.8.5 Constraints

With SMS, the gradient in water potential is constrained between 0 and the range of soil potential between parameters for stomata fully open and closed (Equation 9). The upper constraint caps the gradient in water potential when soil potential reaches the value for stomata fully open ( $\psi_o$  = -0.65 MPa for BET). Darcy’s Law predicts that the gradient in water potential would continue to increase until saturation matric potential. The lower constraint caps the gradient in water potential at zero, disallowing negative gradients. However, reversed water fluxes, caused by positive gradients in water potential from root to soil, have been observed in the field [*Burgess et al.*, 1998]. Both constraints are eschewed with PHS.

## 6 Conclusion

The PHS configuration of the CLM5 is, to our knowledge, the first Earth System Model with a representation of plant water potential running in its default configuration. In this paper, we have described the model implementation, and illustrated a comparison of the model dynamics for a tropical rainforest site subjected to water limitation, given that prediction of rainforest responses to drought is one of the key uncertainties in the ESM predictions [Huntingford *et al.*, 2013]. Overall, the new model behaviour differs from the default configuration in ways that are expected, given its structural properties, and in many cases, provides better correspondence with the observations than the default structure.

In this paper, however, we do not undertake a comprehensive assessment of which model structure performs better, given the substantial parametric uncertainty in both models, and the dependence on numerous other features of the CLM external to water stress representation that contribute to model-observation divergences - in this case in particular, the overestimation of unstressed transpiration by both versions of the model compared to the observations.

In lieu of this type of assessment, we propose that the new PHS model structure 1) is more closely aligned with known plant hydraulics theory, 2) provides significantly improved connections to real-world observational data streams (of leaf and stem water status, sap flow, percent loss conductance) and 3) represents known features of ecohydrological function that the default model cannot capture, including hydraulic redistribution, changes in the depth of water uptake with drought stress, plant embolism impacts on gas exchange and responses of water uptake to changes in leaf:root ratios.

## 7 Acknowledgments

## 8 Figures

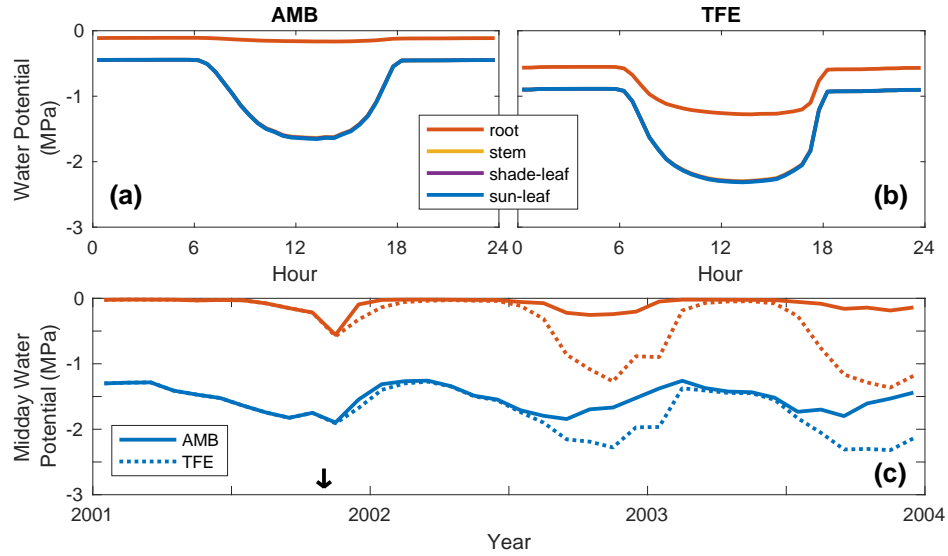


**Figure 3.** (a,b) 2003 dry season diurnal mean of modeled vegetation water potential under ambient and 60% TFE conditions. Curves are drawn for sunlit leaf, shaded leaf, stem, and root water potentials, with the latter three overlapping. (c) Monthly mean midday (12h-14h) vegetation water potential under ambient (solid line) and TFE (dotted line) conditions. Here curves are drawn only for sunlit leaf and root water potential. Note that TFE begins Nov 1, 2001, as indicated by the vertical arrow.



**Figure 4.** 2003 dry season (SON) diurnal mean water stress function for (a) SMS, and (b) PHS. Note that the water stress factor equals 1 when there is no stress and 0 when fully stressed.

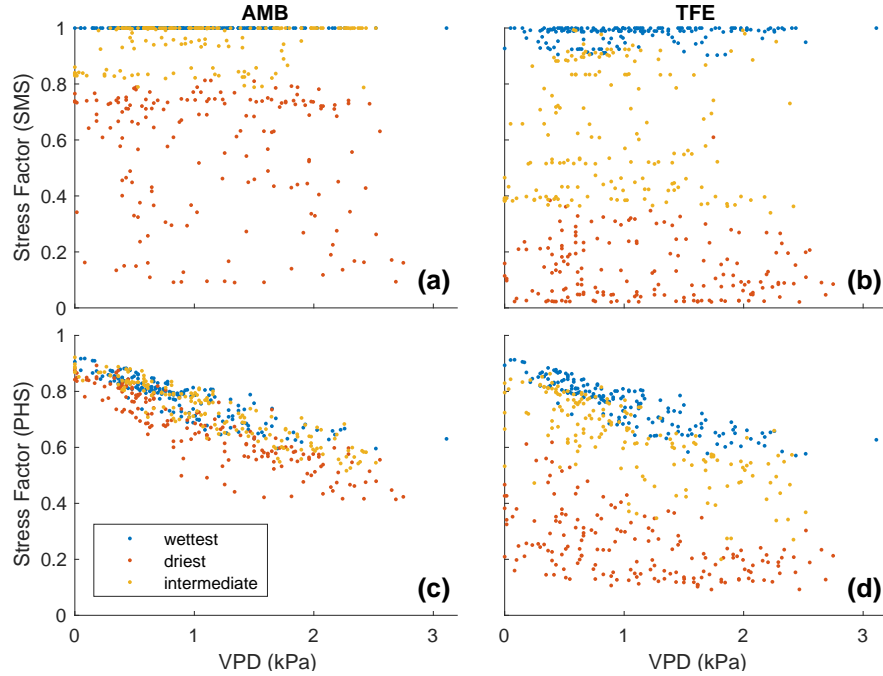


**Figure 5.** Water stress factor versus vapor pressure deficit (2002-2003), constrained to timesteps with downwelling shortwave radiation between 400 and 425 W/m<sup>2</sup> (n=515). Radiation is controlled to highlight the relationship with VPD, the reverse (controlling for VPD) is shown in Figure A.2. For SMS (a,b), data are subdivided based on average soil matric potential, weighted by root fraction. For PHS (c,d), data are subdivided based on predawn (5h) root water potential. Blue dots represent the wettest tercile, yellow dots represent the intermediate tercile, and red dots represent the driest tercile (values defining each tercile are in Table 2).

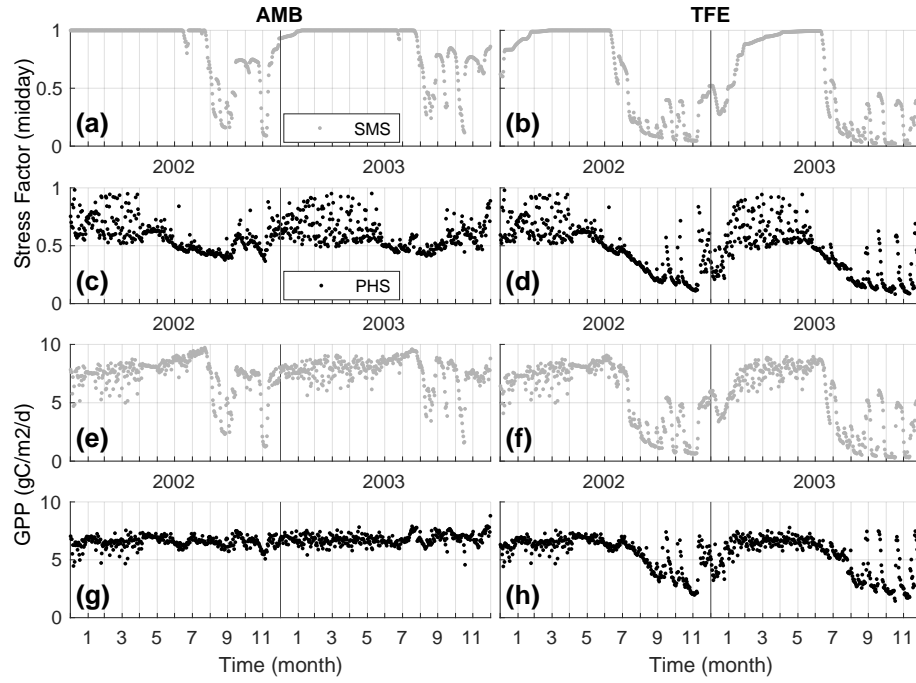


**Figure 6.** Daily stress factor (midday, averaged over 12h-14h) and GPP during 2002-2003 under ambient (left column) and TFE (right right column) conditions. Output from the SMS configuration (a,b,e,f) are plotted with gray color, while output from the PHS configuration (c,d,g,h) are plotted in black.

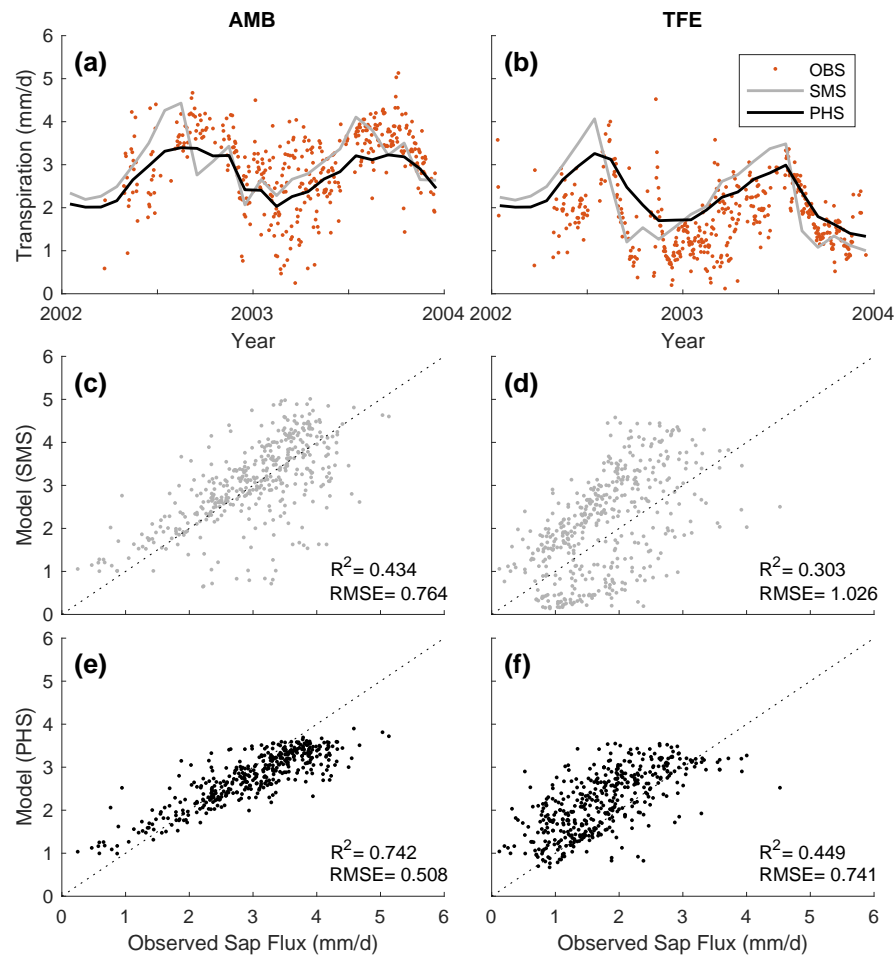


**Figure 7.** (a,b) Monthly mean transpiration over 2002-3 (solid lines), with daily sap flux observations (red dots). (c-f), Model daily transpiration (mm/d) versus observed sap flux.

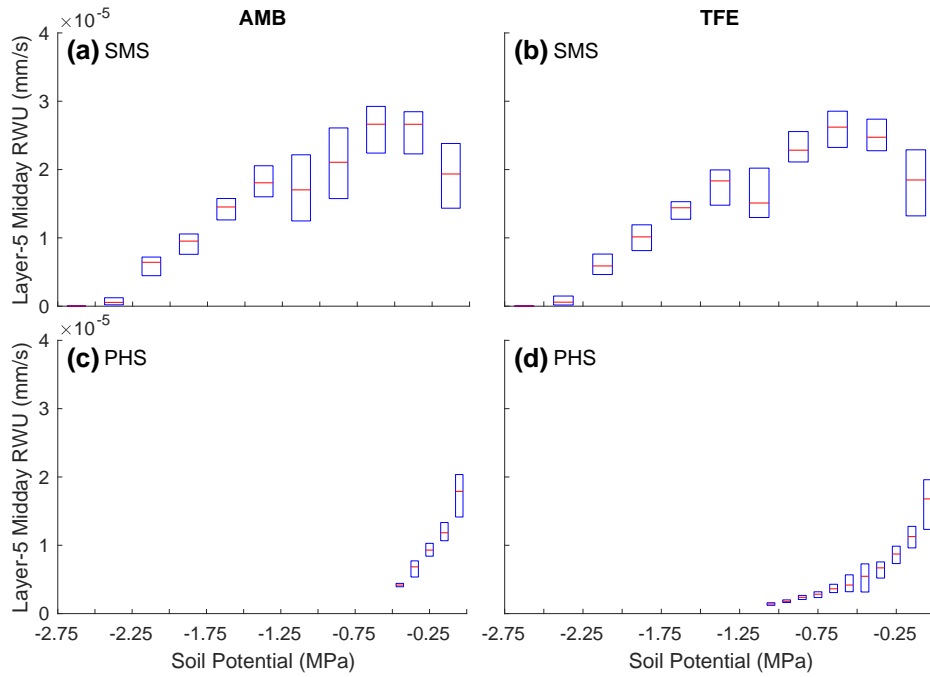


**Figure 8.** Binned boxplot of root water uptake versus soil potential for Soil Layer 5 (2002-3). Red lines mark the median, with boxes spanning the interquartile range. Bin widths are 0.25 MPa for SMS and 0.1 MPa for PHS. Soil Layer 5 is shown, because it is close enough to the surface (20 to 32 cm) to achieve a good range in soil potential, and it has a large root fraction (14.4%, only Soil Layer 6 has a larger root fraction). Only midday (12h-14h) timesteps are used to highlight the relationship with soil potential.



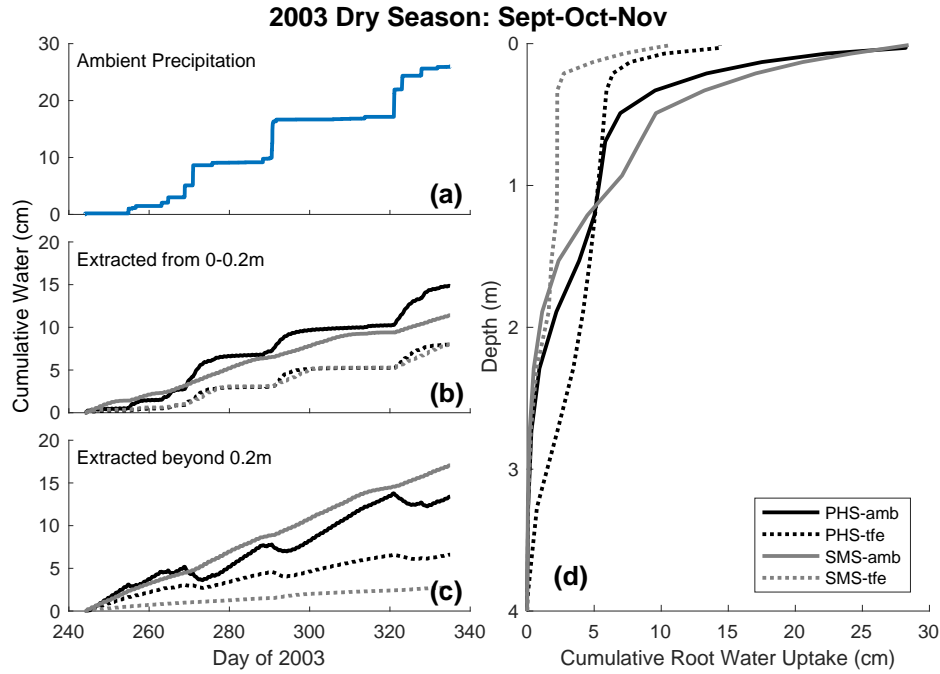


**Figure 9.** 2003 dry season (SON) cumulative root water uptake and precipitation. (a) Cumulative precipitation over time under ambient conditions (b,c) Cumulative water uptake over time from above and below 0.2m, respectively. (d) Cumulative root water uptake with depth.

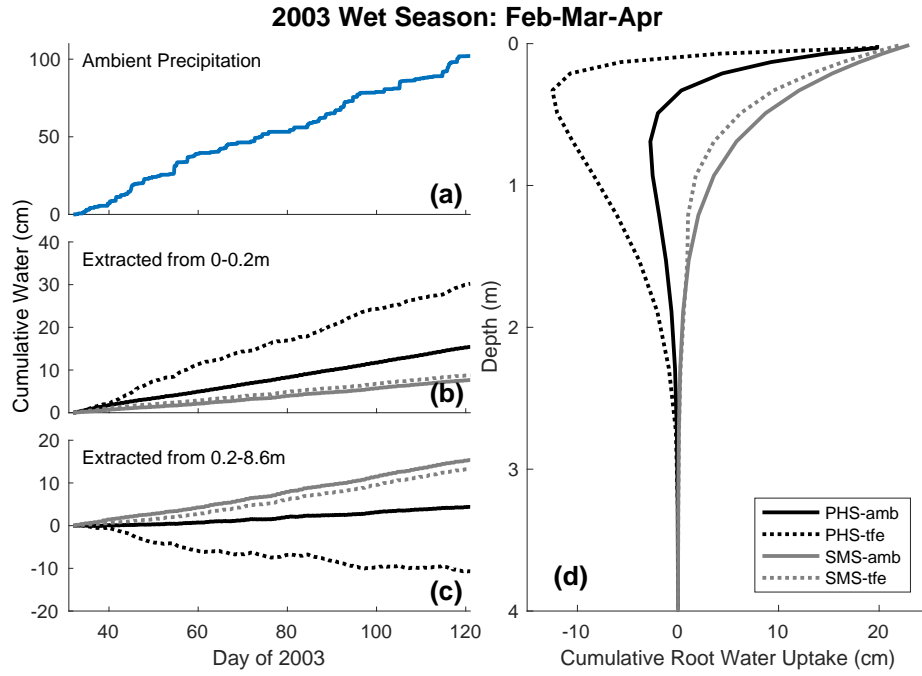


**Figure 10.** 2003 wet season (FMA) cumulative root water uptake and precipitation. (a) Cumulative precipitation over time under ambient conditions (b,c) Cumulative water uptake over time from above and below 0.2m, respectively. (d) Cumulative root water uptake with depth.

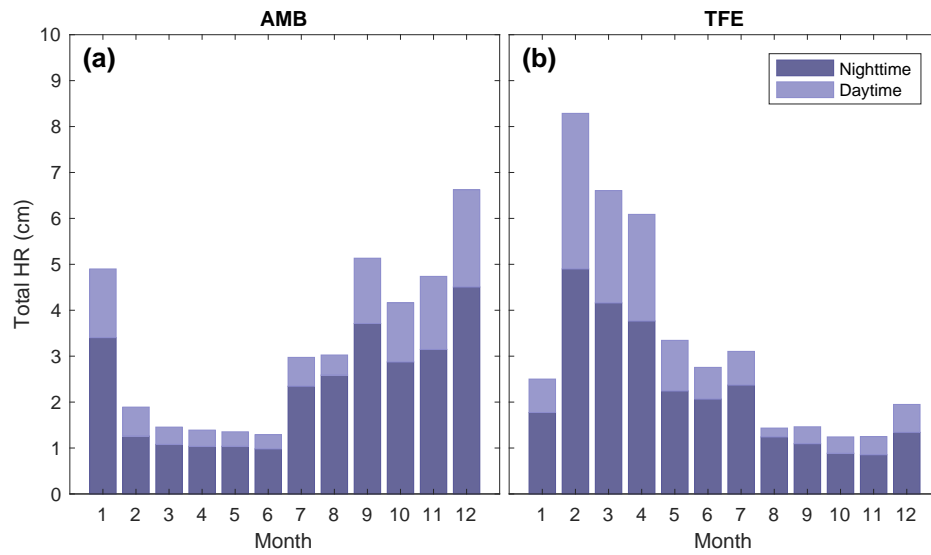


**Figure 11.** Total hydraulic redistribution (cm) by month across 2003. For (a) ambient through-fall conditions, and (b) 60% throughfall exclusion. Darker shading shows portion of HR at night [6pm,6am), lighter shading shows portion of HR during day [6am,6pm). Total HR refers to the sum of all negative root water uptake flows, when water is deposited by roots into a given soil layer.

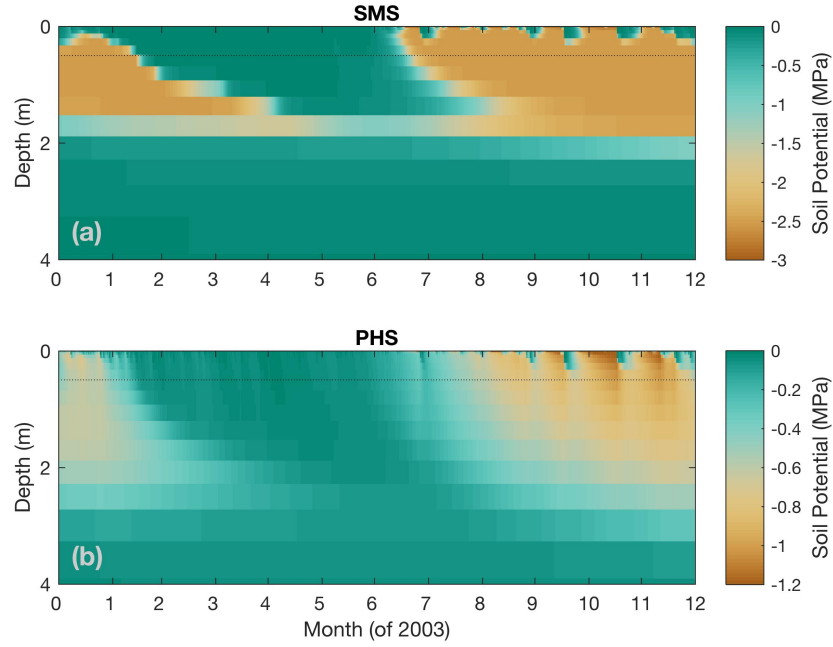


**Figure 12.** Vertical profile of soil water potential (MPa) over time under 60% throughfall exclusion, for (a) SMS, and (b) PHS. Note that color axes are different. SMS soil potential spends long periods at -2.5MPa, which is the value of soil-wilting parameter,  $\psi_c$ . Figure 13 subsets this data at 0.5m depth (dotted line), plotted alongside observations. Soil potential under ambient conditions is shown in Supp Fig A.6.

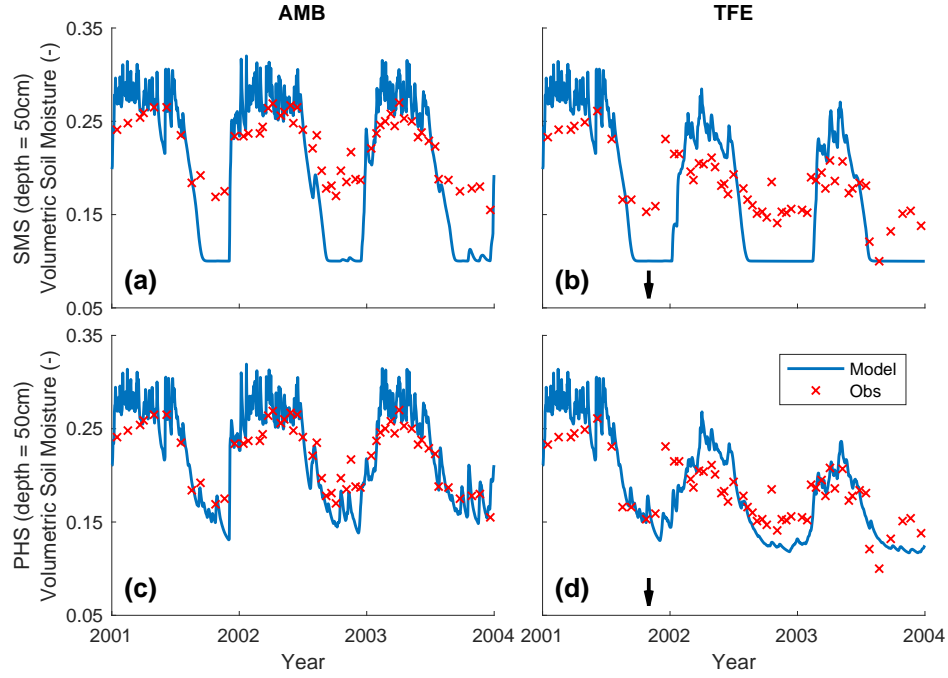


**Figure 13.** Volumetric soil moisture (-) over time under ambient and TFE conditions at depth of 50cm. (a/b) SMS (c/d) PHS. RMSE are 0.048, 0.049, 0.022, and 0.029 [move to plot]. Arrows indicate start of TFE. Figure A.7 shows the same plots at 7 other soil depths.

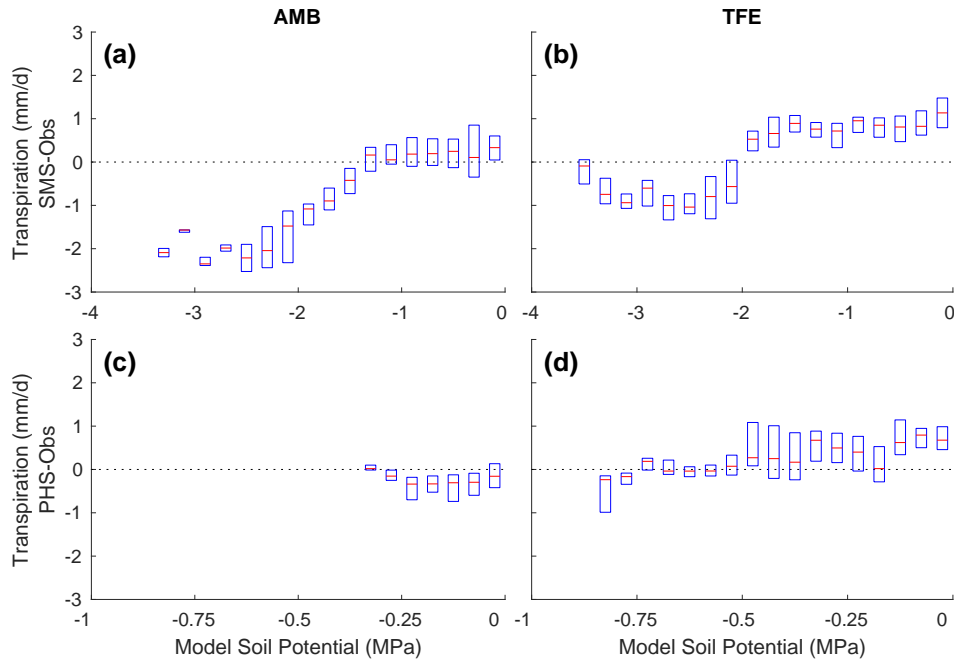
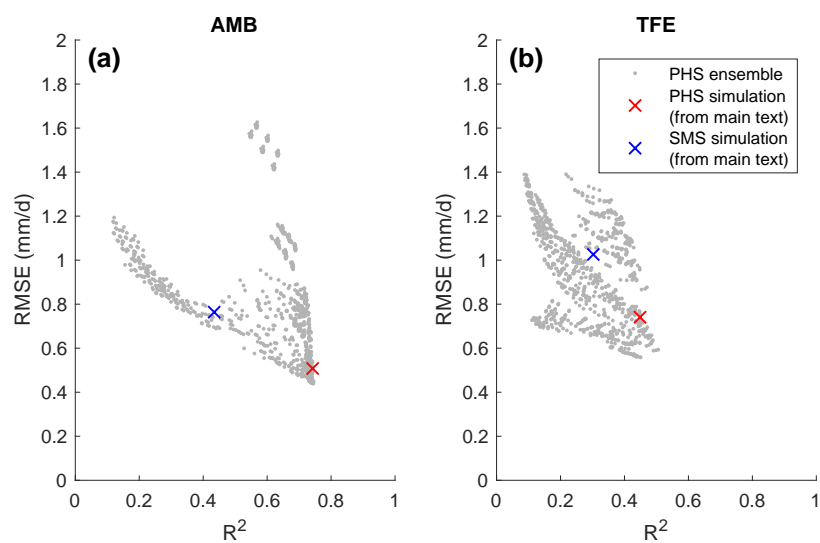


**Figure 14.** Binned boxplot showing the difference between modeled and observed transpiration (mm/d) versus model soil potential. Red lines are drawn at the median, with boxes spanning the interquartile range. The two models use different root water uptake paradigms, from which we define different operators for column effective soil potential. For SMS we average over the soil column weighted by root fraction and over time (daily mean). For PHS we use predawn (5h) root water potential. Bin widths are 0.2 MPa for SMS (a,b) and 0.05 MPa for PHS (c,d); note the different x-axes.

723

## A: Supplementary Figures



724

**Figure A.1.** Parameter tuning exercise.

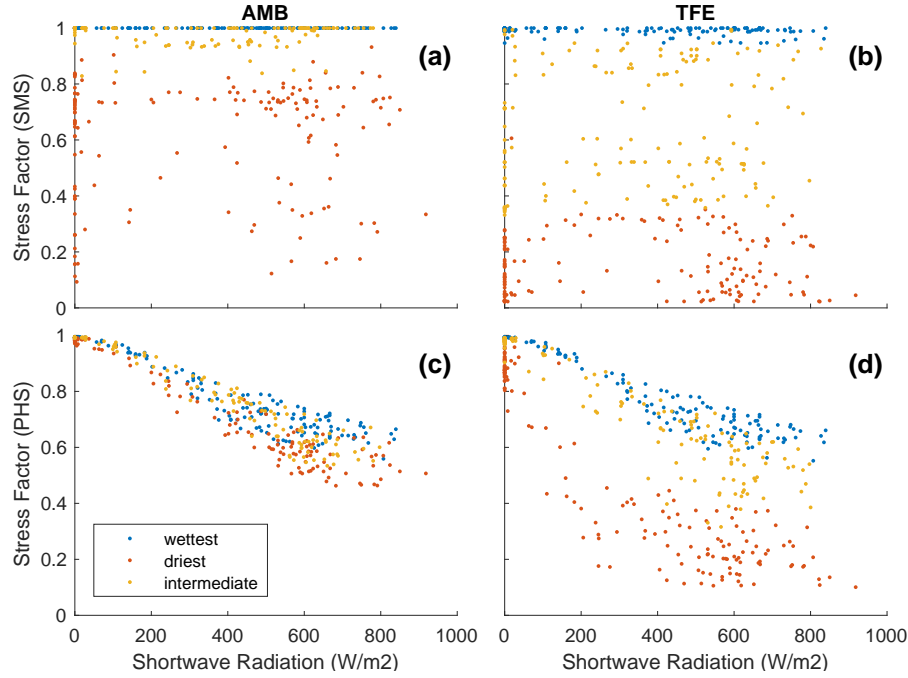


**Figure A.2.** Water stress factor versus downwelling shortwave radiation (2002-2003), for timesteps with VPD between 1 and 1.0559 kPa ( $n=470$ ). VPD is controlled to highlight the relationship with downwelling radiation, the reverse (controlling for radiation) is shown in Figure 5. For SMS (a,b), data are subdivided based on average soil matric potential, weighted by root fraction. For PHS (c,d), data are subdivided based on predawn (5h) root water potential. Blue dots represent the wettest tercile, yellow dots represent the intermediate tercile, and red dots represent the driest tercile.



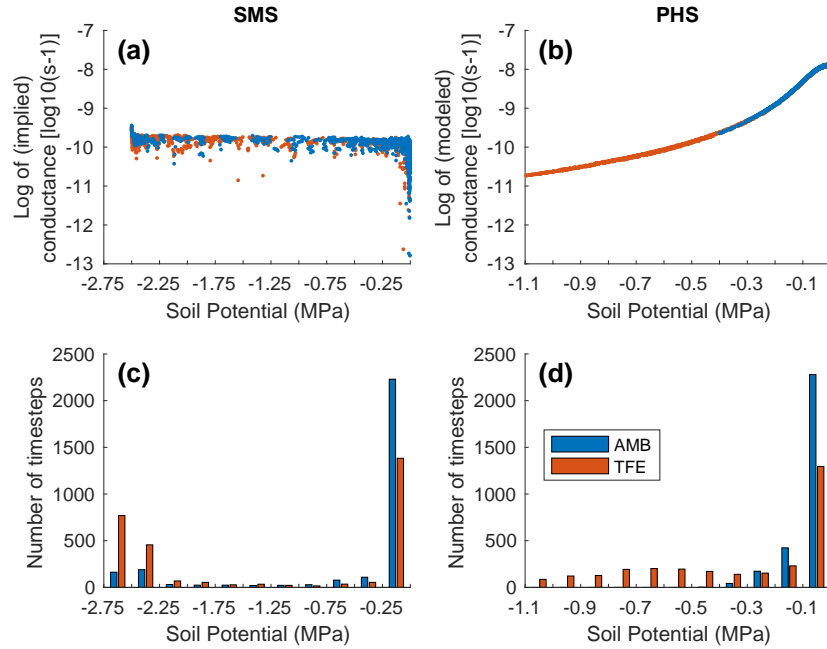
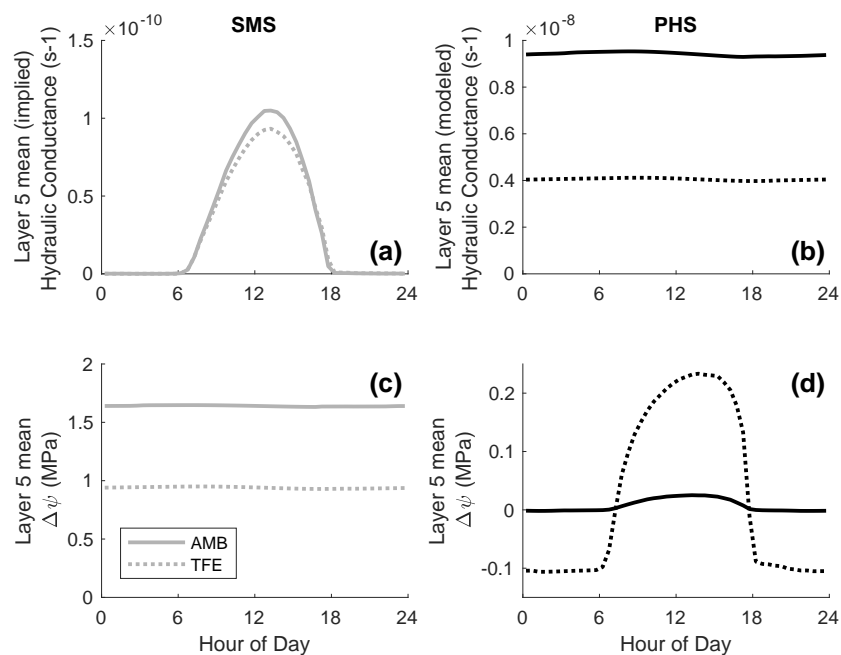
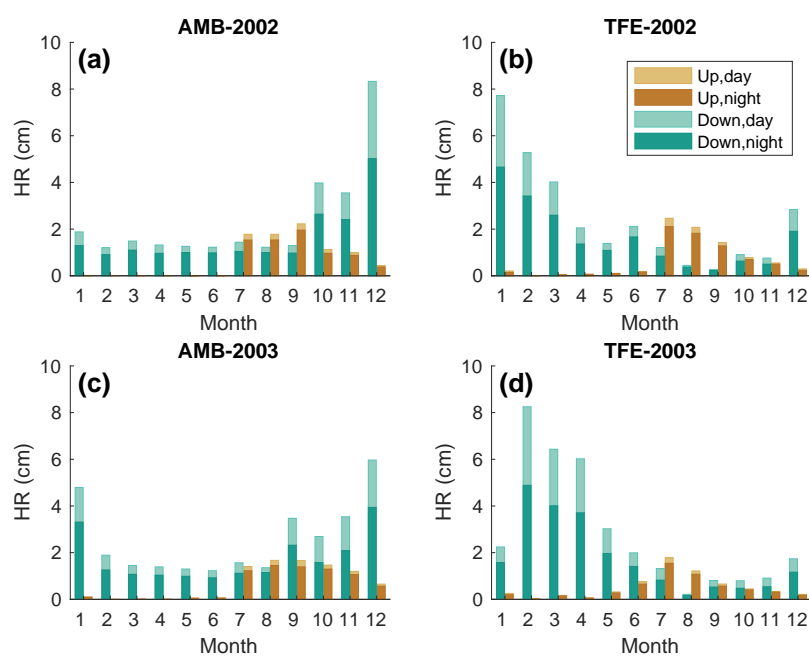


**Figure A.3.** Log of conductance versus soil potential for Soil Layer 5 (2002-3). Only midday (12h-14h) timesteps are shown to emphasize the relationship with soil potential. With SMS, conductance is not modeled explicitly, but rather calculated as  $k=q/\Delta\psi$  (see Section zqz). Beyond 2.5MPa, SMS implied conductance equals 0. PHS conductance captures both root tissue and soil matrix resistances (operating in series).



735

**Figure A.4.** 2003 diurnal mean of Soil Layer 5 conductance and  $\Delta\psi$ , under ambient and TFE conditions.



736

**Figure A.5.** PHS hydraulic distribution during 2003. Alternative version partitioning by direction.

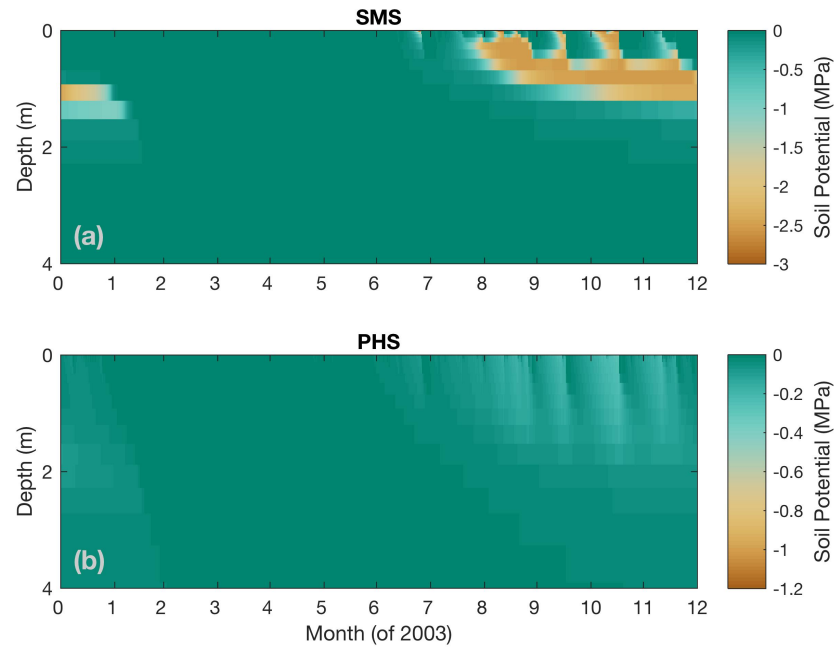


**Figure A.6.** Vertical profile of soil water potential (MPa) through time under ambient through-fall conditions, for (a) PHS, and (b) SMS. Note that color axes are different.

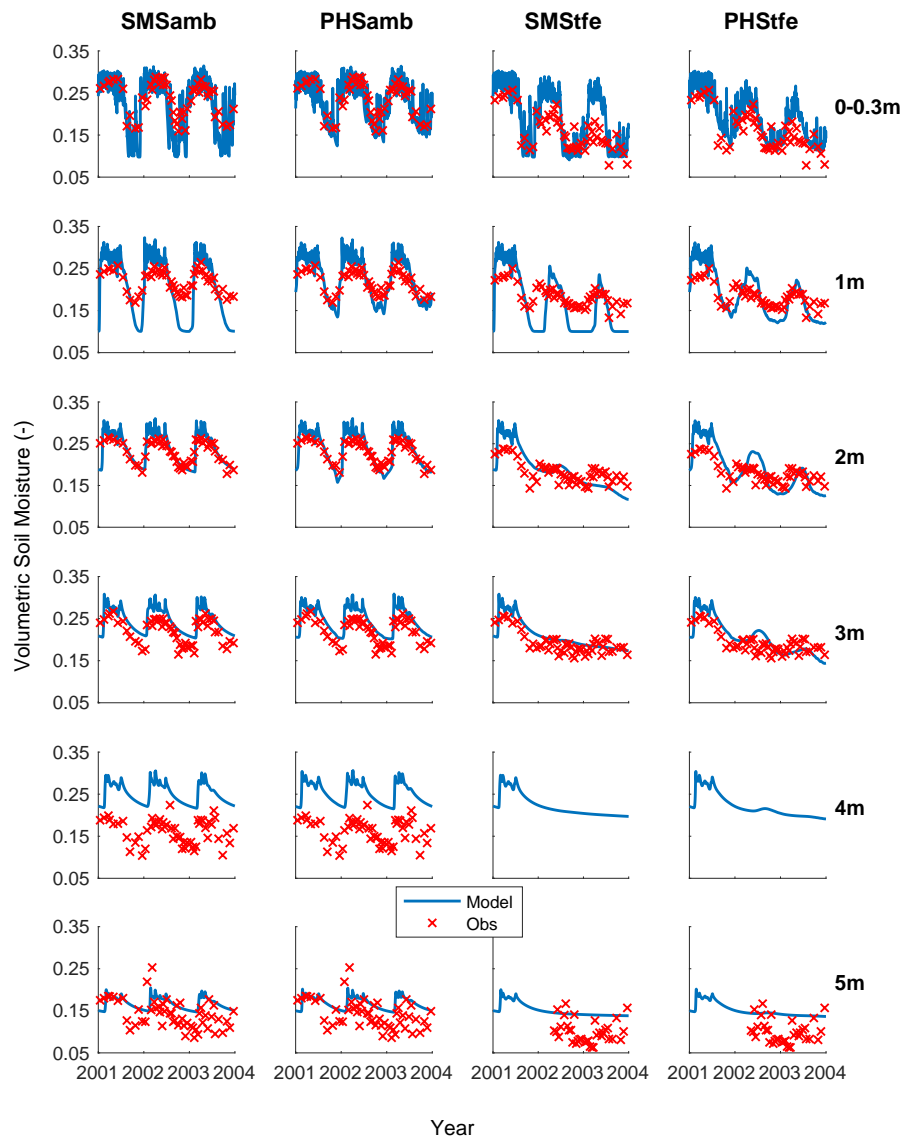


**Figure A.7.** Time series of soil moisture by soil layer. Complements Figure 12

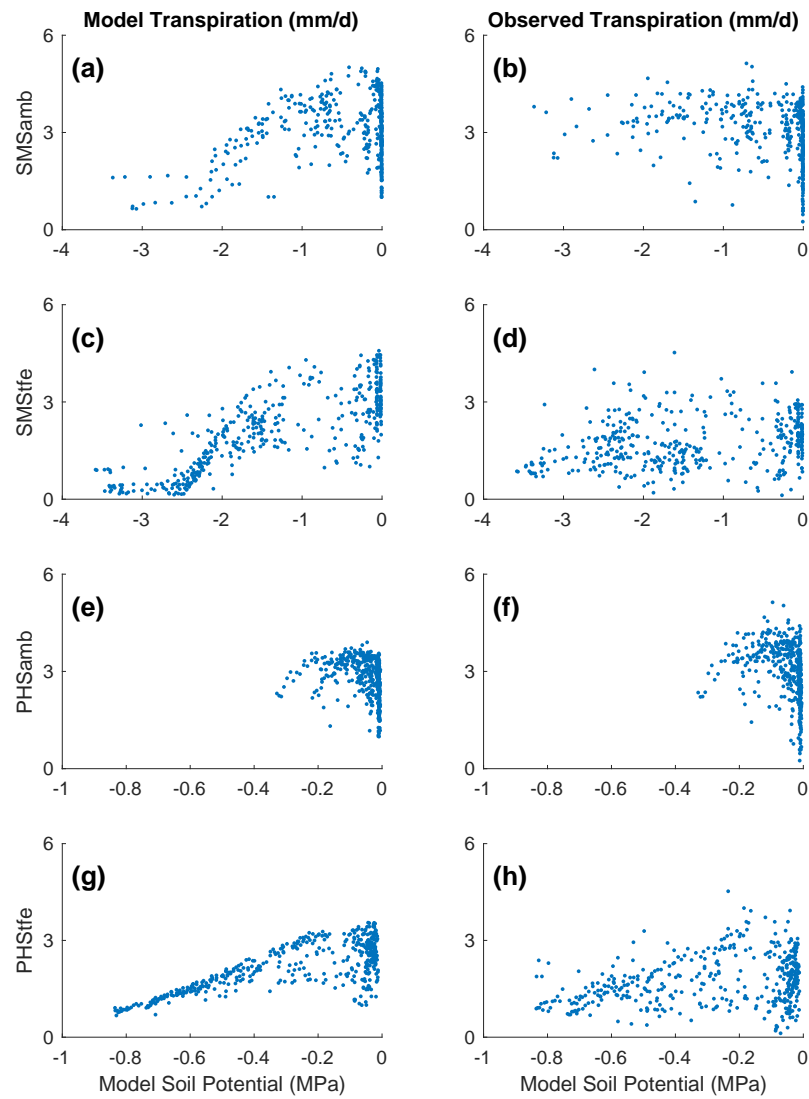


**Figure A.8.** Modeled (left column) and observed (right column) transpiration vs. model soil potential. Complements Figure 14

## B: Appendix to Model Description

### B.1 Details of Water Supply

PHS resolves flow across four different segments, soil-to-root, root-to-stem, stem-to-leaf, and leaf-to-transpiration.

Stem-to-leaf. The area bases are sunlit and shaded leaf area, respectively. Note that gravity is assumed negligible here. Likewise there is no length scaling applied to maximum conductance. Therefore the input parameters for  $k_{1,\max}$  should be conductances ( $s^{-1}$ ).

$$\begin{aligned} q_{1a} &= k_1 \cdot \text{LAI-sun} \cdot (\psi_{\text{stem}} - \psi_{\text{sun-leaf}}) \\ q_{1b} &= k_1 \cdot \text{LAI-shade} \cdot (\psi_{\text{stem}} - \psi_{\text{shade-leaf}}) \end{aligned} \quad (\text{B.1})$$

$$k_1 = k_{1,\max} \cdot f(\psi_{\text{stem}}) \quad (\text{B.2})$$

$$f(\psi) = 2 - \left( \frac{\psi}{p_{50}} \right)^{c_k} \quad (\text{B.3})$$

Root-to-stem. The area basis is stem area index. The parameter is maximum stem xylem conductivity ( $K_{2,\max}$ ). Stem conductance ( $k_2$ ) is the result of scaling maximum conductivity by the tree height ( $h$ ) and applying loss relative to maximum conductance via the vulnerability curve  $f(\psi_{\text{root}})$ .

$$q_2 = k_2 \cdot \text{SAI} \cdot (\psi_{\text{root}} - \psi_{\text{stem}} - \rho g h) \quad (\text{B.4})$$

$$k_2 = \frac{K_{2,\max}}{h} \cdot f(\psi_{\text{root}}) \quad (\text{B.5})$$

Soil-to-root. Area basis is RAI in soil layer  $i$ , which is based on the layer root fraction times the total root area. Total root area we have as the summed stem and leaf area indices multiplied by a relative root area parameter ( $f_{\text{root}}$ ). The vertical root distribution is defined by the layer root fraction ( $r_i$ ), which follows a one-parameter (by PFT) power law decay following *Jackson et al.* [1996].

$$q_{3,i} = k_{3,i} \cdot \text{RAI}_i \cdot (\psi_{\text{soil},i} - \psi_{\text{root}} - \rho g z_i) \quad (\text{B.6})$$

$$\text{RAI}_i = f_{\text{root}} \cdot (\text{SAI} + \text{LAI}) \cdot r_i \quad (\text{B.7})$$

$$k_{3,i} = \frac{k_{r,i} + k_{s,i}}{k_{r,i} \cdot k_{s,i}} \quad (\text{B.8})$$

$$k_{r,i} = \frac{K_{r,\max}}{l_i} f(\psi_{\text{soil},i}) \quad (\text{B.9})$$

$$l_i = z_i + x \quad (\text{B.10})$$

$$k_{s,i} = \frac{K_{s,i}}{d} \quad (\text{B.11})$$

The conductance  $k_{3,i}$  reflects two resistors in series, from soil-to-root ( $k_{s,i}$ ) and through the root tissue ( $k_{r,i}$ ). The root tissue conductance is attenuated via the vulnerability curve framework. The input parameter is maximum root xylem conductivity, on the basis of RAI as defined above. The root conductivity is scaled by the conducting length, which is estimated as the sum of soil layer depth ( $z_i$ ) and average lateral extent ( $x$ , static parameter). The soil conductivity  $K_{s,i}$  is calculated from the layer soil matric potential ( $\psi_s$ ) and soil properties following *Clapp and Hornberger* [1978] as described in *Oleson et al.* [2013]. The soil conductance ( $k_{s,i}$ ) is the result of scaling the conductivity by  $d$ , the distance between roots estimated following *Williams et al.* [1996] and *Bonan et al.* [2014]

The challenge here is obviously getting your head around all the parameters.

## B.2 Details of Water Demand

The CLM5 implementation utilizes the Medlyn stomatal conductance model [Medlyn *et al.*, 2011], while also applying water stress through  $V_{\text{cmax}}$ . Transpiration is calculated reflecting contributions from both stomatal conductance and leaf boundary layer conductance ( $g_b$ ).

$$V_{\text{cmax}} = f_w V_{\text{cmax,ww}} \quad (\text{B.12})$$

$$g_s = g_0 + \left(1 + \frac{g_1}{\sqrt{D}}\right) \frac{A}{C_a} \quad (\text{B.13})$$

$$E_{\text{sun}} = g_{s,\text{sun}} * \rho * \text{VPD} * lai_{\text{sun}} * \left(1 + \frac{g_{s,\text{sun}}}{g_b}\right)^{-1} \quad (\text{B.14})$$

$$E_{\text{shade}} = g_{s,\text{shade}} * \rho * \text{VPD} * lai_{\text{shade}} * \left(1 + \frac{g_{s,\text{shade}}}{g_b}\right)^{-1}$$

At the beginning of a set of PHS iterations, we solve for  $E_{\text{sun,max}}$  and  $E_{\text{shade,max}}$ , by running the stomatal conductance scheme with  $f_w$  set to 1 (no stress). Within each PHS iteration, we do not resolve the full stomatal conductance scheme, but instead consider only the linear attenuation of stomatal conductance by  $f_w$ . Transpiration is attenuated relative to the maximal values according to leaf water potential.

$$E_{\text{sun}} = E_{\text{sun,max}} * 2^{-\left(\frac{\psi_{\text{leaf}}}{\psi_{50}}\right)^{c_k}} \quad (\text{B.15})$$

$$E_{\text{shade}} = E_{\text{shade,max}} * 2^{-\left(\frac{\psi_{\text{leaf}}}{\psi_{50}}\right)^{c_k}}$$

We define  $f_w$  as the ratio of attenuated stomatal conductance ( $g_{s,\text{sun}}$ ,  $g_{s,\text{shade}}$ ) to maximal stomatal conductance ( $g_{s,\text{sun,max}}$ ,  $g_{s,\text{shade,max}}$ ), where  $g_{s,\text{sun,max}}$  and  $g_{s,\text{shade,max}}$  are the stomatal conductance values associated with  $E_{\text{sun,max}}$  and  $E_{\text{shade,max}}$ . As such, the definition in the main text (Equation 13), represents a linear simplification between  $f_w$ , stomatal conductance, and transpiration.

$$f_{w,\text{sun}} = \frac{g_{s,\text{sun}}}{g_{s,\text{sun,max}}} \quad (\text{B.16})$$

$$f_{w,\text{shade}} = \frac{g_{s,\text{shade}}}{g_{s,\text{shade,max}}}$$

After each PHS iteration, we compute  $g_{s,\text{sun}}$  and  $g_{s,\text{shade}}$  via Equations B.12 and B.12 (which involves iterating for intercellular  $\text{CO}_2$  concentration). We then update  $g_{s,\text{sun,max}}$  and  $g_{s,\text{shade,max}}$  to achieve consistency between equations (B.14) and (B.15). At this point  $g_{s,\text{sun,max}}$  and  $g_{s,\text{shade,max}}$  no longer refer to the values associated with  $f_w = 1$ , but rather also incorporate the non-linearity between  $g_s$  and  $f_w$ . The PHS iteration continues to convergence of  $f_w$  (see Figure B.1). The numerics have proven to be stable in practice, but future versions may aim to better integrate PHS within the stomatal conductance scheme to improve the coherence of Equations 13 and B.16.

$$g_{s,\text{sun,max}} = \frac{g_{s,\text{sun}}}{f_{w,\text{sun}}} \quad (\text{B.17})$$

$$g_{s,\text{shade,max}} = \frac{g_{s,\text{shade}}}{f_{w,\text{shade}}}$$



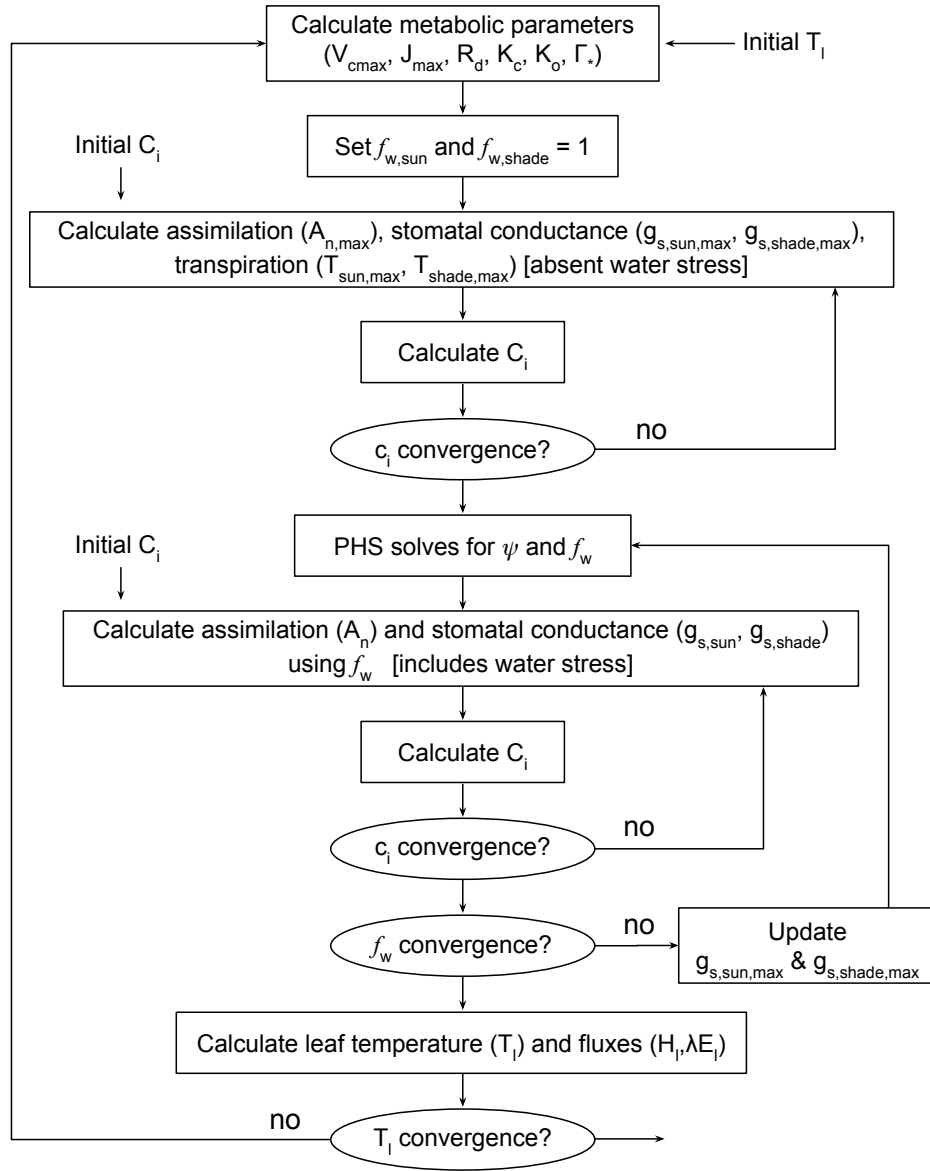


**Figure B.1.** Flow chart of PHS iterative solution

### B.3 Details of Water Potential Solution

The continuity of water flow through the system yields four equations

$$\begin{aligned}
 E_{sun} &= q_{1a} \\
 E_{shade} &= q_{1b} \\
 q_{1a} + q_{1b} &= q_2 \\
 q_2 &= \sum_{i=1}^{nlevsoi} q_{3,i}
 \end{aligned} \tag{B.18}$$

We seek the set of vegetation water potential values (four unknowns),

$$\psi = \begin{bmatrix} \psi_{sunleaf} \\ \psi_{shadeleaf} \\ \psi_{stem} \\ \psi_{root} \end{bmatrix} \tag{B.19}$$

that satisfies these equations, as forced by the soil moisture and atmospheric state.

Each flux on the schematic can be represented in terms of the relevant water potentials.

Defining the transpiration fluxes:

$$\begin{aligned}
 E_{sun} &= E_{sun,max} \cdot 2^{-\left(\frac{\psi_{sunleaf}}{p50_e}\right)^{c_k}} \\
 E_{shade} &= E_{shade,max} \cdot 2^{-\left(\frac{\psi_{shadeleaf}}{p50_e}\right)^{c_k}}
 \end{aligned} \tag{B.20}$$

Defining the water supply fluxes:

$$\begin{aligned}
 q_{1a} &= k_{1a,max} \cdot 2^{-\left(\frac{\psi_{stem}}{p50_1}\right)^{c_k}} \cdot LAI_{sun} \cdot (\psi_{stem} - \psi_{sunleaf}) \\
 q_{1b} &= k_{1b,max} \cdot 2^{-\left(\frac{\psi_{stem}}{p50_1}\right)^{c_k}} \cdot LAI_{shade} \cdot (\psi_{stem} - \psi_{shadeleaf}) \\
 q_2 &= \frac{k_{2,max}}{z_2} \cdot 2^{-\left(\frac{\psi_{root}}{p50_2}\right)^{c_k}} \cdot SAI \cdot (\psi_{root} - \psi_{stem} - \Delta\psi_z) \\
 q_{soil} &= \sum_{i=1}^{nlevsoi} q_{3,i} = \sum_{i=1}^{nlevsoi} k_{3,i} \cdot RAI \cdot (\psi_{soil,i} - \psi_{root} + \Delta\psi_{z,i})
 \end{aligned} \tag{B.21}$$

We're looking to find the vector  $\psi$  that fits with soil and atmospheric forcings while satisfying water flow continuity. Due to the model non-linearity, we use a linearized explicit approach, iterating with Newton's method. The initial guess is the solution for  $\psi$  (vector) from the previous time step. The general framework, from iteration  $m$  to  $m + 1$  is:

$$\begin{aligned}
 q^{m+1} &= q^m + \frac{\delta q}{\delta \psi} \Delta\psi \\
 \psi^{m+1} &= \psi^m + \Delta\psi
 \end{aligned} \tag{B.22}$$

So for our first flux balance equation, at iteration  $m + 1$ , we have:

$$E_{sun}^{m+1} = q_{1a}^{m+1} \quad (B.23)$$

Which can be linearized to:

$$E_{sun}^m + \frac{\delta E_{sun}}{\delta \psi} \Delta \psi = q_{1a}^m + \frac{\delta q_{1a}}{\delta \psi} \Delta \psi \quad (B.24)$$

And rearranged to be:

$$\frac{\delta q_{1a}}{\delta \psi} \Delta \psi - \frac{\delta E_{sun}}{\delta \psi} \Delta \psi = E_{sun}^m - q_{1a}^m \quad (B.25)$$

And for the other 3 flux balance equations:

$$\begin{aligned} \frac{\delta q_{1b}}{\delta \psi} \Delta \psi - \frac{\delta E_{sha}}{\delta \psi} \Delta \psi &= E_{sha}^m - q_{1b}^m \\ \frac{\delta q_2}{\delta \psi} \Delta \psi - \frac{\delta q_{1a}}{\delta \psi} \Delta \psi - \frac{\delta q_{1b}}{\delta \psi} \Delta \psi &= q_{1a}^m + q_{1b}^m - q_2^m \\ \frac{\delta q_{soil}}{\delta \psi} \Delta \psi - \frac{\delta q_2}{\delta \psi} \Delta \psi &= q_2^m - q_{soil}^m \end{aligned} \quad (B.26)$$

Putting all four together in matrix form:

$$\begin{bmatrix} \frac{\delta q_{1a}}{\delta \psi} - \frac{\delta E_{sun}}{\delta \psi} \\ \frac{\delta q_{1b}}{\delta \psi} - \frac{\delta E_{sha}}{\delta \psi} \\ \frac{\delta q_2}{\delta \psi} - \frac{\delta q_{1a}}{\delta \psi} - \frac{\delta q_{1b}}{\delta \psi} \\ \frac{\delta q_{soil}}{\delta \psi} - \frac{\delta q_2}{\delta \psi} \end{bmatrix} \Delta \psi = \begin{bmatrix} E_{sun}^m - q_{1a}^m \\ E_{sha}^m - q_{1b}^m \\ q_{1a}^m + q_{1b}^m - q_2^m \\ q_2^m - q_{soil}^m \end{bmatrix} \quad (B.27)$$

Now to expand the left-hand side, from vector  $\psi$  to the four distinct plant water potential nodes, noting that many derivatives are zero (e.g.  $\frac{\delta E_{sun}}{\delta \psi_{sha}} = 0$ )

Introducing the notation:  $A \Delta \psi = b$

$$\Delta \psi = \begin{bmatrix} \Delta \psi_{sunleaf} \\ \Delta \psi_{shadeleaf} \\ \Delta \psi_{stem} \\ \Delta \psi_{root} \end{bmatrix} \quad (B.28)$$

$$A = \begin{bmatrix} \frac{\delta q_{1a}}{\delta \psi_{sun}} - \frac{\delta E_{sun}}{\delta \psi_{sun}} & 0 & \frac{\delta q_{1a}}{\delta \psi_{stem}} & 0 \\ 0 & \frac{\delta q_{1b}}{\delta \psi_{sha}} - \frac{\delta E_{sha}}{\delta \psi_{sha}} & \frac{\delta q_{1b}}{\delta \psi_{stem}} & 0 \\ -\frac{\delta q_{1a}}{\delta \psi_{sun}} & -\frac{\delta q_{1b}}{\delta \psi_{sha}} & \frac{\delta q_2}{\delta \psi_{stem}} - \frac{\delta q_{1a}}{\delta \psi_{stem}} - \frac{\delta q_{1b}}{\delta \psi_{stem}} & \frac{\delta q_2}{\delta \psi_{root}} \\ 0 & 0 & -\frac{\delta q_2}{\delta \psi_{stem}} & \frac{\delta q_{soil}}{\delta \psi_{root}} - \frac{\delta q_2}{\delta \psi_{root}} \end{bmatrix} \quad (B.29)$$

$$b = \begin{bmatrix} E_{sun}^m - q_{b1}^m \\ E_{sha}^m - q_{b2}^m \\ q_{b1}^m + q_{b2}^m - q_{stem}^m \\ q_{stem}^m - q_{soil}^m \end{bmatrix} \quad (B.30)$$

Now we compute all the entries for  $A$  and  $b$  based on the soil moisture and maximum transpiration forcings and can solve to find:

$$\Delta\psi = A^{-1}b \quad (B.31)$$

$$\psi_{m+1} = \psi_m + \Delta\psi \quad (B.32)$$

We iterate until  $b \rightarrow 0$ , signifying water flux balance through the system. The result is a final set of water potentials ( $\psi_{root}$ ,  $\psi_{xylem}$ ,  $\psi_{shadeleaf}$ ,  $\psi_{sunleaf}$ ) satisfying non-divergent water flux through the system.

#### B.4 Parameter tuning exercise

We used a factorial design to create 972 ensemble members based on the parameter values below. We ran PHS simulations under both AMB and TFE conditions. All simulations used the same initial conditions, which were the result of a previous simulation. We evaluated the ensemble members based on the fit to sap flux observations, selecting that which maximized  $R_{amb}^2 + R_{tfe}^2 - RMSE_{amb} - RMSE_{tfe}$  (Supp Fig A.1).

Stem conductivity,  $k_{max}$ : 2e-8, 4e-8, 8e-8 s<sup>-1</sup>  
 Root conductivity,  $k_{r,max}$ : 2e-9, 6e-8, 18e-9 s<sup>-1</sup>  
 Root and stem vulnerability  $\psi_{50}$ : -1.75, -2.25, -2.75 MPa  
 Stomatal  $\psi_{50}$ : above plus either 0 or 0.5MPa  
 Vulnerability shape parameter,  $c_k$ : 2.95, 3.95, 5.45 (unitless)  
 Medlyn slope,  $g_1$ : 6, 7 kPa<sup>0.5</sup>  
 Rooting depth parameter,  $\beta$ : 0.95, 0.98, 0.993 (unitless)

#### Acknowledgments

= enter acknowledgments here =

#### References

- Allen, C. D., A. K. Macalady, H. Chenchouni, D. Bachelet, N. McDowell, M. Vennetier, T. Kitzberger, A. Rigling, D. D. Breshears, E. T. Hogg, P. Gonzalez, R. Fensham, Z. Zhang, J. Castro, N. Demidova, J.-H. Lim, G. Allard, S. W. Running, A. Semerci, and N. Cobb (2010), A global overview of drought and heat-induced tree mortality reveals emerging climate change risks for forests, *Forest Ecology and Management*, 259(4), 660–684, doi:https://doi.org/10.1016/j.foreco.2009.09.001.
- Anderegg, W. R. L. (2015a), Spatial and temporal variation in plant hydraulic traits and their relevance for climate change impacts on vegetation, *New Phytologist*, 205(3), 1008–1014, doi:10.1111/nph.12907.
- Anderegg, W. R. L., J. M. Kane, and L. D. L. Anderegg (2013a), Consequences of widespread tree mortality triggered by drought and temperature stress, *Nature Climate Change*, 3(1), 30–36.
- Anderegg, W. R. L., L. Plavcová, L. D. L. Anderegg, U. G. Hacke, J. A. Berry, and C. B. Field (2013b), Drought's legacy: multiyear hydraulic deterioration underlies widespread

- 878 aspen forest die-off and portends increased future risk, *Global Change Biology*, 19(4),  
879 1188–1196, doi:10.1111/gcb.12100.
- 880 Anderegg, W. R. L., C. Schwalm, F. Biondi, J. J. Camarero, G. Koch, M. Litvak, K. Ogle,  
881 J. D. Shaw, E. Shevliakova, A. P. Williams, A. Wolf, E. Ziaco, and S. Pacala (2015b), Per-  
882 vasive drought legacies in forest ecosystems and their implications for carbon cycle mod-  
883 els, *Science*, 349(6247), 528–532, doi:10.1126/science.aab1833.
- 884 Anderegg, W. R. L., A. Wolf, A. Arango-Velez, B. Choat, D. J. Chmura, S. Jansen, T. Kolb,  
885 S. Li, F. Meinzer, P. Pita, V. Resco de Dios, J. S. Sperry, B. T. Wolfe, and S. Pacala (2017),  
886 Plant water potential improves prediction of empirical stomatal models, *PLOS ONE*,  
887 12(10), 1–17, doi:10.1371/journal.pone.0185481.
- 888 Bartlett, M. K., T. Klein, S. Jansen, B. Choat, and L. Sack (2016), The correlations and se-  
889 quence of plant stomatal, hydraulic, and wilting responses to drought, *Proceedings of the*  
890 *National Academy of Sciences*, 113(46), 13,098–13,103, doi:10.1073/pnas.1604088113.
- 891 Bohrer, G., H. Mourad, T. A. Laursen, D. Drewry, R. Avissar, D. Poggi, R. Oren, and G. G.  
892 Katul (2005), Finite element tree crown hydrodynamics model (fetch) using porous me-  
893 dia flow within branching elements: A new representation of tree hydrodynamics, *Water*  
894 *Resources Research*, 41(11), doi:10.1029/2005WR004181.
- 895 Bonan, G. B. (2008), Forests and climate change: Forcings, feedbacks, and the climate bene-  
896 fits of forests, *Science*, 320(5882), 1444–1449, doi:10.1126/science.1155121.
- 897 Bonan, G. B., P. J. Lawrence, K. W. Oleson, S. Levis, M. Jung, M. Reichstein, D. M.  
898 Lawrence, and S. C. Swenson (2011), Improving canopy processes in the Commu-  
899 nity Land Model version 4 (CLM4) using global flux fields empirically inferred from  
900 FLUXNET data, *Journal of Geophysical Research*, 116, doi:10.1029/2010JG001593.
- 901 Bonan, G. B., M. Williams, R. A. Fisher, and K. W. Oleson (2014), Modeling stomatal con-  
902 ductance in the earth system: linking leaf water-use efficiency and water transport along  
903 the soil-plant-atmosphere continuum, *Geoscientific Model Development*, 7(5), 2193–2222,  
904 doi:10.5194/gmd-7-2193-2014.
- 905 Bouda, M., and J. E. Saiers (2017), Dynamic effects of root system architecture improve root  
906 water uptake in 1-d process-based soil-root hydrodynamics, *Advances in Water Resources*,  
907 110, 319 – 334, doi:https://doi.org/10.1016/j.advwatres.2017.10.018.
- 908 Boyer, J. S. (1967), Leaf water potentials measured with a pressure chamber, *Plant Physiol-*  
909 *ogy*, 42(1), 133–137, doi:10.1104/pp.42.1.133.
- 910 Brooks, J. R., F. C. Meinzer, J. M. Warren, J.-C. Domec, and R. Coulombe (2006), Hydraulic  
911 redistribution in a douglas-fir forest: lessons from system manipulations, *Plant, Cell &*  
912 *Environment*, 29(1), 138–150, doi:10.1111/j.1365-3040.2005.01409.x.
- 913 Burgess, S. S. O., M. A. Adams, N. C. Turner, and C. K. Ong (1998), The redistribution of  
914 soil water by tree root systems, *Oecologia*, 115(3), 306–311, doi:10.1007/s004420050521.
- 915 Cai, G., J. Vanderborcht, M. Langensiepen, A. Schnepf, H. Hüging, and H. Vereecken  
916 (2018), Root growth, water uptake, and sap flow of winter wheat in response to differ-  
917 ent soil water conditions, *Hydrology and Earth System Sciences*, 22(4), 2449–2470, doi:  
918 10.5194/hess-22-2449-2018.
- 919 Cai, W., S. Borlace, M. Lengaigne, P. Van Rensch, M. Collins, G. Vecchi, A. Timmermann,  
920 A. Santoso, M. J. Mcphaden, L. Wu, M. H. England, G. Wang, E. Guilyardi, and F.-f. Jin  
921 (2014), Increasing frequency of extreme El Niño events due to greenhouse warming, *Nat-*  
922 *ure Climate Change*, 4(2), 111–116.
- 923 Celia, M. A., E. T. Bouloutas, and R. L. Zarba (1990), A general mass-conservative numer-  
924 ical solution for the unsaturated flow equation, *Water Resources Research*, 26(7), 1483–  
925 1496, doi:10.1029/WR026i007p01483.
- 926 Choat, B., S. Jansen, T. J. Brodribb, H. Cochard, S. Delzon, R. Bhaskar, S. J. Bucci, T. S.  
927 Feild, S. M. Gleason, U. G. Hacke, A. L. Jacobsen, F. Lens, H. Maherali, J. Martínez-  
928 Vilalta, S. Mayr, M. Mencuccini, P. J. Mitchell, A. Nardini, J. Pittermann, R. B. Pratt, J. S.  
929 Sperry, M. Westoby, I. J. Wright, and A. E. Zanne (2012), Global convergence in the vul-  
930 nerability of forests to drought, *Nature*, 491(7426), 752–5.

- Christoffersen, B. O., M. Gloor, S. Fauset, N. M. Fyllas, D. R. Galbraith, T. R. Baker, B. Kruijt, L. Rowland, R. A. Fisher, O. J. Binks, S. Sevanto, C. Xu, S. Jansen, B. Choat, M. Mencuccini, N. G. McDowell, and P. Meir (2016), Linking hydraulic traits to tropical forest function in a size-structured and trait-driven model (tfs v.1-hydro), *Geoscientific Model Development*, 9(11), 4227–4255, doi:10.5194/gmd-9-4227-2016.
- Clapp, R. B., and G. M. Hornberger (1978), Empirical equations for some soil hydraulic properties, *Water Resources Research*, 14(4), 601–604, doi:10.1029/WR014i004p00601.
- Collatz, G., J. Ball, C. Grivet, and J. A. Berry (1991), Physiological and environmental regulation of stomatal conductance, photosynthesis and transpiration: a model that includes a laminar boundary layer, *Agricultural and Forest Meteorology*, 54(2), 107 – 136, doi: [http://dx.doi.org/10.1016/0168-1923\(91\)90002-8](http://dx.doi.org/10.1016/0168-1923(91)90002-8).
- Couvreur, V., J. Vanderborght, and M. Javaux (2012), A simple three-dimensional macroscopic root water uptake model based on the hydraulic architecture approach, *Hydrology and Earth System Sciences*, 16(8), 2957–2971, doi:10.5194/hess-16-2957-2012.
- da Costa, A. C., D. B. Metcalfe, C. E. Doughty, A. A. de Oliveira, G. F. Neto, M. C. da Costa, J. de Athaydes Silva Junior, L. E. Aragão, S. Almeida, D. R. Galbraith, L. M. Rowland, P. Meir, and Y. Malhi (2014), Ecosystem respiration and net primary productivity after 8–10 years of experimental through-fall reduction in an eastern Amazon forest, *Plant Ecology & Diversity*, 7(1–2), 7–24, doi:10.1080/17550874.2013.798366.
- da Costa, A. C. L., D. Galbraith, S. Almeida, B. Takeshi, T. Portela, M. da Costa, J. ao de Athaydes Silva Junior, A. P. Braga, P. H. L. de Gonçalves, A. A. de Oliveira, R. Fisher, O. L. Phillips, D. B. Metcalfe, P. Levy, and P. Meir (2010), Effect of 7 yr of experimental drought on vegetation dynamics and biomass storage of an eastern amazonian rainforest, *The New Phytologist*, 187(3), 579–591.
- Dai, A. (2013), Increasing drought under global warming in observations and models, *Nature Climate Change*, 3(1), 52–58.
- Dai, Y., R. E. Dickinson, and Y.-P. Wang (2004), A two-big-leaf model for canopy temperature, photosynthesis, and stomatal conductance, *Journal of Climate*, 17(12), 2281–2299, doi:10.1175/1520-0442(2004)017<2281:ATMFCT>2.0.CO;2.
- De Kauwe, M. G., J. Kala, Y.-S. Lin, A. J. Pitman, B. E. Medlyn, R. A. Duursma, G. Abramowitz, Y.-P. Wang, and D. G. Miralles (2015), A test of an optimal stomatal conductance scheme within the CABLE land surface model, *Geoscientific Model Development*, 8(2), 431–452, doi:10.5194/gmd-8-431-2015.
- De Kauwe, M. G., B. E. Medlyn, J. Knauer, and C. A. Williams (2017), Ideas and perspectives: how coupled is the vegetation to the boundary layer?, *Biogeosciences*, 14(19), 4435–4453, doi:10.5194/bg-14-4435-2017.
- Domec, J.-C., J. S. King, A. Noormets, E. Treasure, M. J. Gavazzi, G. Sun, and S. G. McNulty (2010), Hydraulic redistribution of soil water by roots affects whole-stand evapotranspiration and net ecosystem carbon exchange, *The New Phytologist*, 187(1), 171–183, doi:10.1111/j.1469-8137.2010.03245.x.
- Drake, J., S. Power, R. Duursma, B. Medlyn, M. Aspinwall, B. Choat, D. Creek, D. Eamus, C. Maier, S. Pfautsch, R. Smith, M. Tjoelker, and D. Tissue (2017), Stomatal and non-stomatal limitations of photosynthesis for four tree species under drought: A comparison of model formulations, *Agricultural and Forest Meteorology*, 247, 454 – 466, doi: <https://doi.org/10.1016/j.agrformet.2017.08.026>.
- Egea, G., A. Verhoef, and P. L. Vidale (2011), Towards an improved and more flexible representation of water stress in coupled photosynthesis-stomatal conductance models, *Agricultural and Forest Meteorology*, 151(10), 1370 – 1384, doi: <https://doi.org/10.1016/j.agrformet.2011.05.019>.
- Entekhabi, D., E. G. Njoku, P. E. O'Neill, K. H. Kellogg, W. T. Crow, W. N. Edelstein, J. K. Entin, S. D. Goodman, T. J. Jackson, J. Johnson, J. Kimball, J. R. Piepmeier, R. D. Koster, N. Martin, K. C. McDonald, M. Moghaddam, S. Moran, R. Reichle, J. C. Shi, M. W. Spencer, S. W. Thurman, L. Tsang, and J. V. Zyl (2010), The soil moisture active passive (smap) mission, *Proceedings of the IEEE*, 98(5), 704–716, doi:

- 10.1109/JPROC.2010.2043918.
- Epila, J., N. J. De Baerdemaeker, L. L. Vergeynst, W. H. Maes, H. Beeckman, and K. Steppe (2017), Capacitive water release and internal leaf water relocation delay drought-induced cavitation in African *Maesopsis eminii*, *Tree Physiology*, 37(4), 481–490, doi: 10.1093/treephys/tpw128.
- Farquhar, G. D., S. von Caemmerer, and J. A. Berry (1980), A biochemical model of photosynthetic CO<sub>2</sub> assimilation in leaves of C<sub>3</sub> species, *Planta*, 149(1), 78–90, doi: 10.1007/BF00386231.
- Ficklin, D. L., and K. A. Novick (2017), Historic and projected changes in vapor pressure deficit suggest a continental-scale drying of the United States atmosphere, *Journal of Geophysical Research: Atmospheres*, 122(4), 2061–2079, doi:10.1002/2016JD025855.
- Fisher, R. A., M. Williams, R. L. Do Vale, A. L. Da Costa, and P. Meir (2006), Evidence from Amazonian forests is consistent with isohydric control of leaf water potential, *Plant, Cell & Environment*, 29(2), 151–165, doi:10.1111/j.1365-3040.2005.01407.x.
- Fisher, R. A., M. Williams, A. L. D. Costa, Y. Malhi, R. F. D. Costa, S. Almeida, and P. Meir (2007), The response of an Eastern Amazonian rain forest to drought stress: results and modelling analyses from a throughfall exclusion experiment, *Global Change Biology*, 13(11), 2361–2378, doi:10.1111/j.1365-2486.2007.01417.x.
- Fisher, R. A., M. Williams, M. de Lourdes Ruivo, A. L. de Costa, and P. Meir (2008), Evaluating climatic and soil water controls on evapotranspiration at two Amazonian rainforest sites, *Agricultural and Forest Meteorology*, 148(6), 850 – 861, doi: https://doi.org/10.1016/j.agrformet.2007.12.001.
- Flexas, J., J. Bota, F. Loreto, G. Cornic, and T. D. Sharkey (2004), Diffusive and metabolic limitations to photosynthesis under drought and salinity in c3 plants, *Plant Biology*, 6(3), 269–279, doi:10.1055/s-2004-820867.
- Flexas, J., M. Ribas-Carbó, J. Bota, J. Galmés, M. Henkle, S. Martínez-Cañellas, and H. Medrano (2006), Decreased rubisco activity during water stress is not induced by decreased relative water content but related to conditions of low stomatal conductance and chloroplast CO<sub>2</sub> concentration, *New Phytologist*, 172(1), 73–82, doi:10.1111/j.1469-8137.2006.01794.x.
- Flexas, J., M. M. Barbour, O. Brendel, H. M. Cabrera, M. Carriquian, A. Dñaz-Espejo, C. Douthe, E. Dreyer, J. P. Ferrio, J. Gago, A. Gallá, J. Galmás, N. Kodama, H. Medrano, ÅIJlo Niinemets, J. J. Peguero-Pina, A. Pou, M. Ribas-Carbás, M. Tomàs, T. Tosens, and C. R. Warren (2012), Mesophyll diffusion conductance to co<sub>2</sub>: An unappreciated central player in photosynthesis, *Plant Science*, 193-194, 70 – 84, doi: https://doi.org/10.1016/j.plantsci.2012.05.009.
- Franks, P. J., P. L. Drake, and R. H. Froend (2007), Anisohydric but isohydrodynamic: seasonally constant plant water potential gradient explained by a stomatal control mechanism incorporating variable plant hydraulic conductance, *Plant, Cell & Environment*, 30(1), 19–30, doi:10.1111/j.1365-3040.2006.01600.x.
- Friedlingstein, P., M. Meinshausen, V. K. Arora, C. D. Jones, A. Anav, S. K. Liddicoat, and R. Knutti (2014), Uncertainties in CMIP5 climate projections due to carbon cycle feedbacks, *Journal of Climate*, 27(2), 511–526.
- Fu, R., L. Yin, W. Li, P. A. Arias, R. E. Dickinson, L. Huang, S. Chakraborty, K. Fernandes, B. Liebmann, R. Fisher, and R. B. Myneni (2013), Increased dry-season length over southern Amazonia in recent decades and its implication for future climate projection, *Proceedings of the National Academy of Sciences of the United States of America*, 110(45), 18,110–18,115.
- Gentine, P., D. Entekhabi, A. Chehbouni, G. Boulet, and B. Duchemin (2007), Analysis of evaporative fraction diurnal behaviour, *Agricultural and Forest Meteorology*, 143(1), 13 – 29, doi:https://doi.org/10.1016/j.agrformet.2006.11.002.
- Gentine, P., D. Entekhabi, and J. Polcher (2011), The diurnal behavior of evaporative fraction in the soil–vegetation–atmospheric boundary layer continuum, *Journal of Hydrometeorology*, 12(6), 1530–1546, doi:10.1175/2011JHM1261.1.



- Gentine, P., M. Guérin, M. Uriarte, N. G. McDowell, and W. T. Pockman (2016), An allometry-based model of the survival strategies of hydraulic failure and carbon starvation, *Ecohydrology*, 9(3), 529–546, doi:10.1002/eco.1654.
- Grant, J., J.-P. Wigneron, R. D. Jeu, H. Lawrence, A. Mialon, P. Richaume, A. A. Bitar, M. Drusch, M. van Marle, and Y. Kerr (2016), Comparison of SMOS and AMSR-E vegetation optical depth to four MODIS-based vegetation indices, *Remote Sensing of Environment*, 172, 87 – 100, doi:https://doi.org/10.1016/j.rse.2015.10.021.
- Green, J. K., A. G. Konings, S. H. Alemohammad, J. Berry, D. Entekhabi, J. Kolassa, J.-E. Lee, and P. Gentine (2017), Regionally strong feedbacks between the atmosphere and terrestrial biosphere, *Nature Geoscience*, 10(6), 410–414, doi:10.1038/ngeo2957.
- Harley, P. C., R. B. Thomas, J. F. Reynolds, and B. R. Strain (1992), Modelling photosynthesis of cotton grown in elevated co<sub>2</sub>, *Plant Cell Environment*, 15(3), 271–282, doi:10.1111/j.1365-3040.1992.tb00974.x.
- Holbrook, N. M., E. T. Ahrens, M. J. Burns, and M. A. Zwieniecki (2001), In vivo observation of cavitation and embolism repair using magnetic resonance imaging, *Plant Physiology*, 126(1), 27–31, doi:10.1104/pp.126.1.27.
- Huntingford, C., P. Zelazowski, D. Galbraith, L. M. Mercado, S. Sitch, R. Fisher, M. Lomas, A. P. Walker, C. D. Jones, B. B. Booth, Y. Malhi, D. Hemming, G. Kay, P. Good, S. L. Lewis, O. L. Phillips, O. K. Atkin, J. Lloyd, E. Gloor, J. Zaragoza-castells, P. Meir, R. Betts, P. P. Harris, C. Nobre, J. Marengo, and P. M. Cox (2013), Simulated resilience of tropical rainforests to co<sub>2</sub>-induced climate change, *Nature Geoscience*, 6(4), 268–273.
- Jackson, R. B., J. Canadell, J. R. Ehleringer, H. A. Mooney, O. E. Sala, and E. D. Schulze (1996), A global analysis of root distributions for terrestrial biomes, *Oecologia*, 108(3), 389–411, doi:10.1007/BF00333714.
- Jackson, R. B., J. S. Sperry, and T. E. Dawson (2000), Root water uptake and transport: using physiological processes in global predictions, *Trends in Plant Science*, 5(11), 482 – 488, doi:https://doi.org/10.1016/S1360-1385(00)01766-0.
- Jinyun, T., R. W. J., and N. Jie (), Incorporating root hydraulic redistribution in clm4.5: Effects on predicted site and global evapotranspiration, soil moisture, and water storage, *Journal of Advances in Modeling Earth Systems*, 7(4), 1828–1848, doi:10.1002/2015MS000484.
- Joetzjer, E., C. Delire, H. Douville, P. Ciais, B. Decharme, R. Fisher, B. Christoffersen, J. C. Calvet, A. C. L. da Costa, L. V. Ferreira, and P. Meir (2014), Predicting the response of the Amazon rainforest to persistent drought conditions under current and future climates: a major challenge for global land surface models, *Geoscientific Model Development*, 7(6), 2933–2950, doi:10.5194/gmd-7-2933-2014.
- Kattge, J., S. D. Åz, S. Lavorel, I. C. Prentice, P. Leadley, G. B. ÅNisch, E. Garnier, M. Westoby, P. B. Reich, I. J. Wright, J. H. C. Cornelissen, C. Violle, S. P. Harrison, P. M. Van Bodegom, M. ReichSTEIN, B. J. Enquist, N. A. Soudzilovskaia, D. D. Ackerly, M. Anand, O. Atkin, M. Bahn, T. R. Baker, D. Baldocchi, R. Bekker, C. C. Blanco, B. Blonder, W. J. Bond, R. Bradstock, D. E. Bunker, F. Casanoves, J. Cavender-Bares, J. Q. Chambers, F. S. Chapin Iii, J. Chave, D. Coomes, W. K. Cornwell, J. M. Craine, B. H. Dobrin, L. Duarte, W. Durka, J. Elser, G. Esser, M. Estiarte, W. F. Fagan, J. Fang, F. FernÅNdez-MÅLNdez, A. Fidelis, B. Finegan, O. Flores, H. Ford, D. Frank, G. T. Freschet, N. M. Fyllas, R. V. Gallagher, W. A. Green, A. G. Gutierrez, T. Hickler, S. I. Higgins, J. G. Hodgson, A. Jalili, S. Jansen, C. A. Joly, A. J. Kerkhoff, D. Kirkup, K. Kitajima, M. Kleyer, S. Klotz, J. M. H. Knops, K. Kramer, I. KÅIJHn, H. Kurokawa, D. Laughlin, T. D. Lee, M. Leishman, F. Lens, T. Lenz, S. L. Lewis, J. Lloyd, J. LusiÅÅ, F. Louault, S. Ma, M. D. MaHECHA, P. MaNNING, T. MaSSAD, B. E. Medlyn, J. Messier, A. T. Moles, S. C. MÅIJLler, K. Nadrowski, S. Naeem, Å. Ninemets, S. NÅÜllerT, A. NÅIJSke, R. Ogaya, J. Oleksyn, V. G. Onipchenko, Y. Onoda, J. OrdoÅŠez, G. Overbeck, W. A. Ozinga, S. PatiÅŠO, S. Paula, J. G. Pausas, J. PeÅŠUellas, O. L. Phillips, V. Pillar, H. Poorter, L. Poorter, P. Poschlod, A. Prinzing, R. Proulx, A. Rammig, S. Reinsch, B. Reu, L. Sack, B. Salgado-Negret, J. Sardans, S. Shiodera, B. Shipley, A. Siefert, E. Sosinski, J.-F. Soussana, E. Swaine, N. Swenson, K. Thompson,



- P. Thornton, M. Waldram, E. Weiher, M. White, S. White, S. J. Wright, B. Yguel, S. Zahle, A. E. Zanne, and C. Wirth (2011), Try a global database of plant traits, *Global Change Biology*, 17(9), 2905–2935, doi:10.1111/j.1365-2486.2011.02451.x.
- Klein, T., and S. Niu (2014), The variability of stomatal sensitivity to leaf water potential across tree species indicates a continuum between isohydric and anisohydric behaviours, *Functional Ecology*, 28(6), 1313–1320, doi:10.1111/1365-2435.12289.
- Konings, A. G., and P. Gentine (2017a), Global variations in ecosystem-scale isohydricity, *Global Change Biology*, 23(2), 891–905, doi:10.1111/gcb.13389.
- Konings, A. G., M. Piles, K. Rützer, K. A. McColl, S. K. Chan, and D. Entekhabi (2016), Vegetation optical depth and scattering albedo retrieval using time series of dual-polarized l-band radiometer observations, *Remote Sensing of Environment*, 172, 178 – 189, doi: <https://doi.org/10.1016/j.rse.2015.11.009>.
- Konings, A. G., A. P. Williams, and P. Gentine (2017b), Sensitivity of grassland productivity to aridity controlled by stomatal and xylem regulation, *Nature Geoscience*, 10(4), 284–288, doi:10.1038/ngeo2903.
- Kotowska, M. M., D. Hertel, Y. A. Rajab, H. Barus, and B. Schuldt (2015), Patterns in hydraulic architecture from roots to branches in six tropical tree species from cacao agroforestry and their relation to wood density and stem growth, *Frontiers in Plant Science*, 6, 191, doi:10.3389/fpls.2015.00191.
- Lee, J.-E., R. S. Oliveira, T. E. Dawson, and I. Fung (2005), Root functioning modifies seasonal climate, *Proceedings of the National Academy of Sciences of the United States of America*, 102(49), 17,576–17,581, doi:10.1073/pnas.0508785102.
- Lemordant, L., P. Gentine, A. S. Swann, B. I. Cook, and J. Scheff (2018), Critical impact of vegetation physiology on the continental hydrologic cycle in response to increasing CO<sub>2</sub>, *Proceedings of the National Academy of Sciences*, doi:10.1073/pnas.1720712115.
- Lin, C., P. Gentine, Y. Huang, K. Guan, H. Kimm, and S. Zhou (2018), Diel ecosystem conductance response to vapor pressure deficit is suboptimal and independent of soil moisture, *Agricultural and Forest Meteorology*, 250–251, 24 – 34, doi: <https://doi.org/10.1016/j.agrformet.2017.12.078>.
- Mackay, D. S., D. E. Roberts, B. E. Ewers, J. S. Sperry, N. G. McDowell, and W. T. Pockman (2015), Interdependence of chronic hydraulic dysfunction and canopy processes can improve integrated models of tree response to drought, *Water Resources Research*, 51(8), 6156–6176, doi:10.1002/2015WR017244.
- Manzoni, S., G. Vico, G. Katul, P. A. Fay, W. Polley, S. Palmroth, and A. Porporato (2011), Optimizing stomatal conductance for maximum carbon gain under water stress: a meta-analysis across plant functional types and climates, *Functional Ecology*, 25(3), 456–467, doi:10.1111/j.1365-2435.2010.01822.x.
- Manzoni, S., G. Vico, G. Katul, S. Palmroth, R. B. Jackson, and A. Porporato (2013a), Hydraulic limits on maximum plant transpiration and the emergence of the safety-efficiency trade-off, *New Phytologist*, 198(1), 169–178, doi:10.1111/nph.12126.
- Manzoni, S., G. Vico, S. Palmroth, A. Porporato, and G. Katul (2013b), Optimization of stomatal conductance for maximum carbon gain under dynamic soil moisture, *Advances in Water Resources*, 62, 90 – 105, doi:<https://doi.org/10.1016/j.advwatres.2013.09.020>.
- McDowell, N., C. D. Allen, K. Anderson, P. Brando, R. Brien, J. Chambers, B. Christoffersen, S. Davies, C. Doughty, A. Duque, F. Espirito Santo, R. Fisher, C. G. Fontes, D. Galbraith, D. Goodman, C. Grossiord, H. Hartmann, J. Holm, D. J. Johnson, A. R. Kassim, M. Keller, C. Koven, L. Kueppers, T. Kumagai, Y. Malhi, S. M. McMahon, M. Mencuccini, P. Meir, P. Moorcroft, H. C. Muller, O. L. Phillips, T. Powell, C. A. Sierra, J. Sperry, J. Warren, C. Xu, and X. Xu (2018), Drivers and mechanisms of tree mortality in moist tropical forests, *New Phytologist*, 0(0), doi:10.1111/nph.15027.
- McDowell, N. G., and C. D. Allen (2015), Darcy’s law predicts widespread forest mortality under climate warming, *Nature Climate Change*, 5(7), 669–672.
- McDowell, N. G., R. A. Fisher, C. Xu, J. C. Domec, T. Hultine, D. S. Mackay, J. S. Sperry, A. Boutz, L. Dickman, N. Gehres, J. M. Limousin, A. Macalady, J. Martínez-Vilalta,



- Restaino, C. M., D. L. Peterson, and J. Littell (2016), Increased water deficit decreases douglas fir growth throughout western US forests, *Proceedings of the National Academy of Sciences*, 113(34), 9557–9562, doi:10.1073/pnas.1602384113.
- Restrepo-Coupe, N., N. M. Levine, B. O. Christoffersen, L. P. Albert, J. Wu, M. H. Costa, D. Galbraith, H. Imbuzeiro, G. Martins, A. C. da Araujo, Y. S. Malhi, X. Zeng, P. Moorcroft, and S. R. Saleska (2017), Do dynamic global vegetation models capture the seasonality of carbon fluxes in the amazon basin? A data-model intercomparison, *Global Change Biology*, 23(1), 191–208, doi:10.1111/gcb.13442.
- Rogers, A., B. E. Medlyn, J. S. Dukes, G. Bonan, S. Caemmerer, M. C. Dietze, J. Kattge, A. D. B. Leakey, L. M. Mercado, Å. Niinemets, I. C. Prentice, S. P. Serbin, S. Sitch, D. A. Way, and S. Zaehle (2017), A roadmap for improving the representation of photosynthesis in earth system models, *New Phytologist*, 213(1), 22–42, doi:10.1111/nph.14283.
- Sack, L., P. J. Melcher, M. A. Zwieniecki, and N. M. Holbrook (2002), The hydraulic conductance of the angiosperm leaf lamina: a comparison of three measurement methods, *Journal of Experimental Botany*, 53(378), 2177–2184.
- Scholz, F. G., N. G. Phillips, S. J. Bucci, F. C. Meinzer, and G. Goldstein (2011), Hydraulic capacitance: Biophysics and functional significance of internal water sources, in Meinzer, F.C., Lachenbruch, B., Dawson, T. E. (eds) *Size- and Age-Related Changes in Tree Structure and Function*, pp. 341–361, Springer, Dordrecht.
- Seager, R., A. Hooks, A. P. Williams, B. Cook, J. Nakamura, and N. Henderson (2015), Climatology, variability, and trends in the u.s. vapor pressure deficit, an important fire-related meteorological quantity, *Journal of Applied Meteorology and Climatology*, 54(6), 1121–1141, doi:10.1175/JAMC-D-14-0321.1.
- Sellers, P. J., D. A. Randall, G. J. Collatz, J. A. Berry, C. B. Field, D. A. Dazlich, C. Zhang, G. D. Collelo, and L. Bounoua (1996a), a revised land surface parameterization (sib2) for atmospheric gcms. part i: Model formulation, *Journal of Climate*, 9(4), 676–705, doi:10.1175/1520-0442(1996)009<0676:ARLSPF>2.0.CO;2.
- Sellers, P. J., C. J. Tucker, G. J. Collatz, S. O. Los, C. O. Justice, D. A. Dazlich, and D. A. Randall (1996b), A revised land surface parameterization (sib2) for atmospheric gcms. part ii: The generation of global fields of terrestrial biophysical parameters from satellite data, *Journal of Climate*, 9(4), 706–737, doi:10.1175/1520-0442(1996)009<0706:ARLSPF>2.0.CO;2.
- Sheffield, J., E. F. Wood, and M. L. Roderick (2012), Little change in global drought over the past 60 years, *Nature*, 491(7424), 435–8.
- Simonin, K. A., E. Burns, B. Choat, M. M. Barbour, T. E. Dawson, and P. J. Franks (2015), Increasing leaf hydraulic conductance with transpiration rate minimizes the water potential drawdown from stem to leaf, *Journal of Experimental Botany*, 66(5), 1303–1315, doi:10.1093/jxb/eru481.
- Siqueira, M., G. Katul, and A. Porporato (2008), Onset of water stress, hysteresis in plant conductance, and hydraulic lift: Scaling soil water dynamics from millimeters to meters, *Water Resources Research*, 44(1), W01432, doi:10.1029/2007WR006094.
- Sperry, J. S., and D. M. Love (2015), What plant hydraulics can tell us about responses to climate-change droughts, *New Phytologist*, 207(1), 14–27, doi:10.1111/nph.13354.
- Sperry, J. S., F. R. Adler, G. S. Campbell, and J. P. Comstock (1998), Limitation of plant water use by rhizosphere and xylem conductance: results from a model, *Plant Cell Environment*, 21(4), 347–359, doi:10.1046/j.1365-3040.1998.00287.x.
- Sperry, J. S., U. G. Hacke, R. Oren, and J. P. Comstock (2002), Water deficits and hydraulic limits to leaf water supply, *Plant, Cell & Environment*, 25(2), 251–263, doi:10.1046/j.0016-8025.2001.00799.x.
- Sperry, J. S., M. D. Venturas, W. R. L. Anderegg, M. Mencuccini, D. S. Mackay, Y. Wang, and D. M. Love (2017), Predicting stomatal responses to the environment from the optimization of photosynthetic gain and hydraulic cost, *Plant, Cell & Environment*, 40(6), 816–830, doi:10.1111/pce.12852, pCE-16-0541.R1.

- Thornton, P. E., and N. E. Zimmermann (2007), An improved canopy integration scheme for a land surface model with prognostic canopy structure, *Journal of Climate*, 20(15), 3902–3923, doi:10.1175/JCLI4222.1.
- Trugman, A. T., D. Medvigy, J. S. Mankin, and W. R. L. Anderegg (2018), Soil moisture stress as a major driver of carbon cycle uncertainty, *Geophysical Research Letters*, 45, doi:10.1029/2018GL078131.
- Tyree, M. T., and J. S. Sperry (1988), Do woody plants operate near the point of catastrophic xylem dysfunction caused by dynamic water stress?: Answers from a model, *Plant Physiology*, 88(3), 574–580.
- Tyree, M. T., and J. S. Sperry (1989), Vulnerability of xylem to cavitation and embolism, *Annual Review of Plant Physiology and Plant Molecular Biology*, 40(1), 19–36, doi:10.1146/annurev.pp.40.060189.000315.
- Ukkola, A. M., M. G. D. Kauwe, A. J. Pitman, M. J. Best, G. Abramowitz, V. Haverd, M. Decker, and N. Haughton (2016), Land surface models systematically overestimate the intensity, duration and magnitude of seasonal-scale evaporative droughts, *Environmental Research Letters*, 11(10), 104,012.
- Verhoef, A., and G. Egea (2014), Modeling plant transpiration under limited soil water: Comparison of different plant and soil hydraulic parameterizations and preliminary implications for their use in land surface models, *Agricultural and Forest Meteorology*, 191, 22–32, doi:https://doi.org/10.1016/j.agrformet.2014.02.009.
- Warren, J. M., P. J. Hanson, C. M. Iversen, J. Kumar, A. P. Walker, and S. D. Wullschlegel (2015), Root structural and functional dynamics in terrestrial biosphere models – evaluation and recommendations, *New Phytologist*, 205(1), 59–78, doi:10.1111/nph.13034.
- Williams, A. P., C. D. Allen, A. K. Macalady, D. Griffin, C. A. Woodhouse, D. M. Meko, T. W. Swetnam, S. A. Rauscher, R. Seager, H. Grissino-Mayer, J. S. Dean, E. R. Cook, C. Gangodagamage, M. Cai, and N. G. McDowell (2013), Temperature as a potent driver of regional forest drought stress and tree mortality, *Nature Climate Change*, 3(3), 292–297.
- Williams, M., E. B. Rastetter, D. N. Fernandes, M. L. Goulden, S. C. Wofsy, G. R. Shaver, J. M. Melillo, J. W. Munger, S.-M. Fan, and K. J. Nadelhoffer (1996), Modelling the soil-plant-atmosphere continuum in a quercus stand at harvard forest: the regulation of stomatal conductance by light, nitrogen and soil/plant hydraulic properties, *Plant, Cell & Environment*, 19(8), 911–927, doi:10.1111/j.1365-3040.1996.tb00456.x.
- Williams, M., B. E. Law, P. M. Anthoni, and M. H. Unsworth (2001), Use of a simulation model and ecosystem flux data to examine carbon–water interactions in ponderosa pine., *Tree Physiology*, 21(5), 287 – 298.
- Xu, X., D. Medvigy, J. S. Powers, J. M. Becknell, and K. Guan (2016), Diversity in plant hydraulic traits explains seasonal and inter-annual variations of vegetation dynamics in seasonally dry tropical forests, *New Phytologist*, 212(1), 80–95, doi:10.1111/nph.14009, 2015-20772.
- Zhou, S., R. A. Duursma, B. E. Medlyn, J. W. Kelly, and I. C. Prentice (2013), How should we model plant responses to drought? An analysis of stomatal and non-stomatal responses to water stress, *Agricultural and Forest Meteorology*, 182-183, 204 – 214, doi:https://doi.org/10.1016/j.agrformet.2013.05.009.
- Zhou, S., B. Medlyn, S. Sabaté, D. Sperlich, I. C. Prentice, and D. Whitehead (2014), Short-term water stress impacts on stomatal, mesophyll and biochemical limitations to photosynthesis differ consistently among tree species from contrasting climates, *Tree Physiology*, 34(10), 1035, doi:10.1093/treephys/tpu072.